



UNIVERSITEIT•STELLENBOSCH•UNIVERSITY
jou kennisvennoot • your knowledge partner

The Use of Trajectory Optimisation as a Means to Study Disturbance Rejection in Bipedal Robots

Matthew Swanevelder
19827938

Report submitted in partial fulfilment of the requirements of the module
Project (E) 448 for the degree Baccalaureus in Engineering in the Department of
Electrical and Electronic Engineering at Stellenbosch University.

Supervisor: Mr C. Fisher

November 2020

Acknowledgements

I would like to thank my supervisor Callen Fisher for all the support and feedback he provided me throughout this project. Your dependable input was greatly appreciated and I truly enjoyed working with you. I would also like to thank my family for providing me the opportunity to study at Stellenbosch and for always supporting me with everything I do. Lastly I would like to thank Elizabeth Labuschagne for her continuous support and her assistance in proof reading my report.



UNIVERSITEIT•STELLENBOSCH•UNIVERSITY
jou kennisvennoot • your knowledge partner

Plagiaatverklaring / Plagiarism Declaration

1. Plagiaat is die oorneem en gebruik van die idees, materiaal en ander intellektuele eiendom van ander persone asof dit jou eie werk is.

Plagiarism is the use of ideas, material and other intellectual property of another's work and to present it as my own.

2. Ek erken dat die pleeg van plagiaat 'n strafbare oortreding is aangesien dit 'n vorm van diefstal is.

I agree that plagiarism is a punishable offence because it constitutes theft.

3. Ek verstaan ook dat direkte vertalings plagiaat is.

I also understand that direct translations are plagiarism.

4. Dienooreenkomsdig is alle aanhalings en bydraes vanuit enige bron (ingesluit die internet) volledig verwys (erken). Ek erken dat die woordelikse aanhaal van teks sonder aanhalingstekens (selfs al word die bron volledig erken) plagiaat is.

Accordingly all quotations and contributions from any source whatsoever (including the internet) have been cited fully. I understand that the reproduction of text without quotation marks (even when the source is cited) is plagiarism

5. Ek verklaar dat die werk in hierdie skryfstuk vervat, behalwe waar anders aangedui, my eie oorspronklike werk is en dat ek dit nie vantevore in die geheel of gedeeltelik ingehandig het vir bepunting in hierdie module/werkstuk of 'n ander module/werkstuk nie.

I declare that the work contained in this assignment, except where otherwise stated, is my original work and that I have not previously (in its entirety or in part) submitted it for grading in this module/assignment or another module/assignment.

19827938	
Studentenommer / Student number	Handtekening / Signature
MC Swanevelder	09/11/2020
Voorletters en van / Initials and surname	Datum / Date

Abstract

English

This study investigated the use of trajectory optimisation algorithms in determining optimal disturbance rejection motions for bipedal robots. The investigation included a variety of disturbances that were applied to a biped model and allowing the trajectory optimisation algorithm to choose the optimal response motions for these disturbances. Results were simulated by defining the optimisation problem as a Pyomo model and then solving the model using the IPOPT solver. From analysing the results it was concluded that trajectory optimisation algorithms can be used to assist in identifying and improving disturbance rejection motions in bipedal robots.

Afrikaans

In die studie word navorsing gedoen om te bewys dat trajek-optimalisering gebruik kan word om die reaksie-beweging van tweevootige robotte te verbeter wanneer dit aan 'n steuringskrag blootgestel is. Ondersoek word ingestel deur 'n verskeidenheid steuringskragte uit te oefen op 'n tweevootige robot model en die trajek-optimalisering algoritme te gebruik om die beste reaksie-beweging te kies vir die robot. Resultate was gesimuleer deur die optimaliseringsprobleem te omskep in 'n Pyomo model en die model dan op te los met die IPOPT oplosser. Nadat die resultate ontleed is, was die gevolgtrekking dat trajek-optimalisering wel gebruik kan word om optimale reaksies te indentifiseer vir tweevootige robotte.

Contents

Declaration	ii
Abstract	iii
List of Figures	vi
List of Tables	ix
Nomenclature	x
1. Introduction	1
1.1. Motivation	1
1.2. Aims of Study	1
1.3. Objectives	2
1.4. Research Questions	2
1.5. Scope and limitations	2
1.6. Outline of Report	3
2. Literature Review	4
2.1. Bipedal robots and disturbance forces	4
2.2. Trajectory Optimisation	6
2.3. Disturbance rejection	7
3. Methodology	10
3.1. Modelling	10
3.2. Disturbance forces	11
3.3. Optimisation Model	11
3.4. Trajectory solver	12
3.5. Analysis	13
4. Trajectory Optimisation	15
4.1. Euler-Lagrange dynamics	15
4.2. Transcription	18
4.3. Direct-collocation Method	19
4.3.1. Collocation	19
4.4. Constraints and bounds	21

4.4.1. General coordinates	21
4.4.2. Motor model	22
4.4.3. Contact Implicit Method	23
4.4.4. Terminal conditions	24
5. Results and Analysis	25
5.1. Mid-body disturbances	26
5.2. Head disturbances	31
5.3. Summary	35
6. Analysis and results of biped with added arm	37
7. Conclusion	39
7.1. Summary	39
7.2. Future Work	40
Bibliography	41
A. Project planning schedule	44
B. Outcomes Compliance	45
C. Additional figures	46

List of Figures

2.1. Lateral push test	5
2.2. Uneven terrain test	5
2.3. Zero Moment Point	7
2.4. Capture Region	8
2.5. ARS results	9
3.1. Bipedal models	11
3.2. Modelling components of a Pyomo model	12
3.3. Graphical representation of the process executed by solver	13
3.4. The GRF components used to calculate the moments about CoM	14
4.1. Collocation Method	20
5.1. GRF angles (Test: 2000N applied at the back of the mid-body)	27
5.2. Simulated biped motion with ground reaction forces added (Test: 2000N applied at the back of the mid-body)	27
5.3. Moments about the CoM (Test: 2000N applied at the back of the mid-body)	27
5.4. GRF angles (Test: 500N applied at the back of the mid-body)	28
5.5. Simulated biped motion with ground reaction forces added (Test: 500N applied at the back of the mid-body)	29
5.6. Moments about the CoM (Test: 500N applied at the back of the mid-body)	29
5.7. GRF angles (Test: 500N applied at the front of the mid-body)	30
5.8. Simulated biped motion with ground reaction force added (Test: 500N applied at the front of the mid-body)	31
5.9. Moments about the CoM (Test: 500N applied at the front of the mid-body)	31
5.10. GRF angles (Test: 500N applied at the back of the head)	32
5.11. Simulated biped motion with ground reaction forces added (Test: 500N applied at back of the head)	33
5.12. Moments about the CoM (Test: 500N applied at the back of the head) . .	33
5.13. GRF angles (Test: 500N applied at the front of the head)	33
5.14. Simulated biped motion with ground reaction forces added (Test: 500N applied at the front of the head)	34
5.15. Moments about the CoM (Test: 500N applied at the front of the head) . .	34

5.16. The stability regions for the ground reaction forces identified from the simulated results.	36
6.1. The disturbance response motion and ground reaction forces of the biped with the added arm for nodes [3,4,8,14,17,20]. [Test: 1500N applied at the back of the mid-body]	37
6.2. The disturbance response motion and ground reaction forces of the biped with the added arm for nodes [1,6,8,9,11,16]. [Test: 500N applied at the back of the head]	38
A.1. Planning Schedule	44
B.1. ECSA Exit Level Outcomes	45
C.1. The typical biped response when a 2000N lateral force applied at the back of the mid-body - The biped takes to two steps to recover from disturbance force and comes to rest at $x_f = 0.1226m$	46
C.2. The typical biped response when a 1500N lateral force applied at the back of the mid-body - The biped takes one step to recover from disturbance force and comes to rest at $x_f = 0.0868m$	46
C.3. The typical biped response when a 1000N lateral force applied at the back of the mid-body - The biped takes to one step to recover from disturbance force and comes to rest at $x_f = 0.0731m$	47
C.4. The typical biped response when a 500N lateral force applied at the back of the mid-body - The biped successfully rejects the disturbance without stepping.	47
C.5. The typical biped response when a 400N lateral force applied at the front of the mid-body - The biped steps backward a distance of $0.0187m$ with the left leg and then returns to original position.(note: the biped was facing towards the left when mid-body front tests were conducted)	48
C.6. The typical biped response when a 500N lateral force applied at the front of the mid-body - The biped steps backward a distance of $0.025m$ with the left leg and then returns to original position.(note: the biped was facing towards the left when mid-body front tests were conducted)	48
C.7. The typical biped response when a 500N lateral force applied at the front of the head - The biped takes to one step backwards to recover from disturbance force and comes to rest at $x_f = 0.042m$.(note: the biped was facing towards the left when mid-body front tests were conducted)	49
C.8. Simulated disturbance response motion of the biped with a single link arm added. [Test: 1500N applied at the back of the mid-body]	49

C.9. Ground reaction force angles of the right and left foot for the first six nodes when 1000N lateral force is applied at the back of mid-body.	50
C.10. Ground reaction force angles of the right and left foot for the first six nodes when 1500N lateral force is applied at the back.	50
C.11. Ground reaction force angles of the right and left foot for the first three nodes when no disturbance force is applied.	50
C.12. These figures show the total moment created by the GRF forces about the CoM of the biped over all 30 nodes.	51
C.13. [Test: 300N applied to the back of the head] The two graphs above show the normal distribution and histogram of the moments about the CoM for five different seeds simulated. The moments of all 30 nodes are represented in the graphs.	51
C.14. [Test: 500N applied to the back of the head] The two graphs above show the normal distribution and histogram of the moments about the CoM for five different seeds simulated. The moments of all 30 nodes are represented in the graphs.	51
C.15. [Test: 300N applied to the front of the head] The two graphs above show the normal distribution and histogram of the moments about the CoM for five different seeds simulated. The moments of all 30 nodes are represented in the graphs.	52
C.16. [Test: 500N applied to the front of the head] The two graphs above show the normal distribution and histogram of the moments about the CoM for five different seeds simulated. The moments of all 30 nodes are represented in the graphs.	52

List of Tables

2.1. Disturbances	5
5.1. Disturbance tests simulated on the five-link biped model	25

Nomenclature

Variables and functions

I	Moment of Inertia
q	Generalised Coordinates
u	Applied torques
P_{CoM}	Position vector
T	Kinetic energy
V	Potential energy
g	Gravitational constant
q_0	Generalised Coordinates at node points
h	Time interval between nodes
tt	Total time up to specific node and collocation point
tt_0	Total time up to specific node point
N	Number of node points
i	Node point
j	Collocation point

Acronyms and abbreviations

CoM	Centre of Mass
ZMP	Zero Moment Point
FZMP	Fictitious Zero Moment Point
CoP	Center of Pressure
BoS	Base of Support
DoF	Degrees of Freedom
PYOMO	Python Optimisation Modeling Object
IPOPT	Interior Point Optimiser
GRF	Ground Reaction Force

Chapter 1

Introduction

1.1. Motivation

Interest regarding legged robots has grown increasingly over the last few years with a significant focus being placed on bipedal robots. Legged robots, unlike other robots, have the ability to easily traverse unstructured environments making them a suitable solution for activities such as exploration, inspection tasks and disaster recovery. Bipedal robots are also considered as a viable replacement for certain human occupations because of their ability to emulate human actions with a high degree of success. However, it is important to ensure that these robots can safely interact with humans and perform their tasks efficiently without errors before introduction into the workplace. A major issue with bipeds, when compared to four-legged robots, is the need for more complex balancing systems to allow them to stand upright and prevent them from falling over when they are subjected to disturbances. The manner in which a robot reacts to disturbance forces can play a huge role in how safe and efficiently a robot can perform its tasks. Information and research regarding the typical disturbance forces that a biped should withstand is lacking - specifically the magnitudes, time periods and positions of these forces. It is therefore important to identify a method or criteria that can be used to identify optimal motions of a biped when subjected to a variety of disturbances. It is also important that this concept is scalable to any bipedal robot.

1.2. Aims of Study

Using the motions generated from a trajectory optimisation algorithm, this study aims to identify common trends that can ultimately be used to create a criteria for optimal disturbance responses. Another aim of this study includes determining, with the use of trajectory optimisation, if adding arms to a five-link robot can assist optimal disturbance rejection.

1.3. Objectives

The initial objective of this study was to model the system dynamics for a five-link bipedal robot with the use of Lagrange dynamics. Thereafter, system dynamics were used to define the bipedal robot in an optimisation model. Because it is solely the trajectory optimizer that decides the path of the robot, it was necessary to add constraints and bounds to the optimisation model to reduce the search space. Once the objectives above had been achieved, the biped was simulated. Various disturbance forces were then be applied to the robot and the simulated results were analysed for common trends. The methods used to identify the common trends included observing the ground reaction forces and the moments about the CoM of the biped throughout the simulation. The results of the five-link biped were then be compared to results of a biped with added arms.

1.4. Research Questions

The ultimate goal of this study was to observe and analyse the optimal disturbance rejection motions for a bipedal robot by making use op trajectory optimisation. This goal was divided into the following research questions, namely:

1. Can trajectory optimisation be used as a tool to help identify a criteria for optimal disturbance rejection motions of a bipedal robot?
2. Can it be proven, using trajectory optimisation data, that the adding of arms to five-link bipedal robot can assist disturbance rejection?

1.5. Scope and limitations

The outcome of this study was solely based on data collected from trajectory optimisation simulations. Due to time and cost limitations results were not tested on real hardware. The robot model used is the study was a five-link robot with torque actuators located at the hips and knees. To help reduce the complexity of the problem all simulations were done in the xz-plane and only disturbances applied to the front and back of the biped were considered. When simulating the disturbances it was also assumed that the biped was on a horizontal surface with a friction coefficient of 1. The time constraints of the study meant that the data collected was only sufficient enough to prove the concept of trajectory optimisation being used to help identify optimal disturbance responses.

1.6. Outline of Report

Chapter 2 investigates literature that is related to the focus of the study and provides background on important aspects of the dissertation. These aspects include, bipedal robots and disturbance forces, trajectory optimisation and disturbance rejection.

Chapter 3 provides a broad overview of how the biped was modelled and how the trajectory solver was implemented. It also discusses what disturbance force tests were performed and how the data was analysed to produce results.

Chapter 4 gives a detailed description of the trajectory optimisation algorithm design. This includes the mathematical model design, direct-collocation design and the chosen constraints and bounds of the system.

Chapter 5 provides the analysis of the data collected during the study. The simulated motions, ground reaction force angles and moments about the CoM of the biped were focused on during the analysis.

Chapter 6 includes the results and analysis of the biped with the added arm. The results are compared to results from chapter 5 to show whether the added arm is beneficial to disturbance rejection motions.

Chapter 7 provides a summary of the study and the results obtained. From this a conclusion is drawn and suggestions are made for future work.

Chapter 2

Literature Review

2.1. Bipedal robots and disturbance forces

Legged robots that are inspired by mammals have become a common trend in robot design with prime examples being MIT's robotic cheetah and Boston Dynamic's robotic dog Spot. Humans can also serve as a very good reference for the design of bipedal robots as well as how a biped should react to disturbance forces. Robots that have bodies that resemble humans are referred to has humanoids. [1] The main reasons for humanoid design as discussed in [2] [3] are as follows:

1. Improving functionality of the robot, allowing it to perform better in human environments.
2. For experimental purposes to help the study of bipedal locomotion.
3. Improving cooperation between bipedal robots and humans, as they would be more relatable having human-like characteristics and similar physical capabilities

Basing the bipedal design on human characteristics can help address the complex challenge that this study presents in creating a realistic simulation that will produce results that can assist in real world applications. Important design characteristics could include bounds on the joints, for example the total range of motion for hips and knees, and the dimensions of the robot. The use of a humanoid robot, and comparing it to human responses, also allows an easier identification of what are the typical disturbances the robot should withstand without falling over. There are a variety of methods used to emulate disturbance forces for simulation and testing phases of a humanoid. Popular methods used, as indicated in [4] [5] [6], is to apply a lateral force at different points on the robot's body or to let the robot walk over an uneven terrain. Figures 2.1 and 2.2 indicate how popular robotics company, Boston Dynamics, apply the above-mentioned methods to test their Atlas robot. The real world tests shown below can only be implemented once extensive simulation testing has been done. This poses the challenge of creating disturbance forces in a simulation environment that are realistic and accurately resemble real world disturbances. Experiments done in [4] [5] [6] show that when attempting to simulate a lateral force



Figure 2.1: Lateral push test



Figure 2.2: Uneven terrain test

there are two aspects that should be considered, namely the size of the force and the time duration of the force. Disturbance forces with brief time periods of contact can be viewed as *punching* forces while forces that have longer contact periods can be viewed as *pushing* forces. There is not much research indicating the time differences of a punch force and pushing force. A good approach that can be used to address this problem is to view the disturbance force as an impulse force, which is calculated as the product of the magnitude and time period of the force. The times and disturbance forces used in other bipedal robot studies like [4], [5] and [6] can also assist in developing realistic disturbances. (Refer to Table 2.1) Approximating realistic force sizes can also be done by

Type	Magnitude[N]	Period[s]	Weight of robot[kg]
lateral mid-body	550-650	0.2	93
lateral mid-body	100	0.4	22
lateral mid-body	100	0.2	30

Table 2.1: Typical disturbance forces used in other studies [4] [5] [6]

studying typical forces exerted by humans and scaling these forces to the humanoid being developed. For reference the average push strengths for men and women are roughly 123N and 85N respectively [7], and the average boxer can exert up to 5000N in one punch. [8]

The uneven terrain test can be easily implemented in a two-dimensional simulation with the following methods used in [4] [5] [6]. The first method is to randomise the point of impact height for a set time interval of the simulation and the second, more simpler method, is to add a step to the horizontal surface that the robot is walking across. This study will, however, focus on disturbance forces encountered by a stationary robot and therefore simulating an uneven terrain will not serve as a suitable test. Testing methods will instead focus on applying lateral forces at different points of the stationary robot.

2.2. Trajectory Optimisation

In many robotic applications the motions of the robot are still optimised manually, which is not cost-effective and is susceptible to errors. This has led to a large increase in research regarding algorithms that can be used to calculate the trajectory of robot motions. These algorithms can also be referred to as trajectory planning algorithms. The trajectory planning algorithm provides the trajectories of the robot's joints as a sequence of values for the position, velocity and acceleration. To calculate these values the algorithm uses the geometric path as well as the kinematic and dynamic constraints of the robot. [9] Trajectory optimisation is a form of trajectory planning and is the process of designing a trajectory that minimises, or maximises, some degree of performance while fulfilling the constraints of the system. [10] The purpose of trajectory optimisation in robotics, as indicated in [9], is usually to minimise one or more of the following popular criteria:

- Execution time
- Energy consumption (or actuator effort)
- Jerk

The minimum execution time optimisation is the most commonly used, as it leads to a reduction in manufacturing time and an increase in robot productivity. There is a large variety of techniques used to implement a minimum time function, but most of them fail to consider actuator dynamics which leads to discontinuation in the actuator's torque and accelerations. To counter this problem and improve the smoothness of the trajectory a flexible tolerance method can be implemented to assist the solver and torque bounds can be set. [9]

There are a number of advantages to optimising with respect to energy consumption. These are that it delivers a smoother trajectory, it reduces mechanical stress on actuators as well as the structure of the robot and most importantly it reduces energy usage. This is important because many robots have a limited power supply, for example battery powered robots, and by minimising the energy consumption the operating lifetime of the robot can be increased. Reducing energy consumption can also reduce the cost of the robot as smaller power units are required. [9]

Jerk is the third derivative of position and it can be viewed as the rate of change of acceleration. Optimising with the goal of reducing jerk can help improve trajectory continuity and can also assist in reducing joint positioning errors. The wear and tear of the robots actuators and joints is also mitigated due to the decrease in robot vibration limits. [11]

The purpose of this study was to determine the most energy efficient disturbance rejection motions and therefore the trajectory was optimised to minimise energy consumption (or actuator effort).

2.3. Disturbance rejection

Understanding stability in legged robots is crucial for studying and analysing disturbance rejection of humanoids. Modern robotic designs use the *Zero Moment Point*(ZMP) approach to define the stability in legged robots. If a point exists on the ground where all the horizontal components of the ground reaction moments are equal to zero, it is called the zero moment point. The stability of the robot can determined from the location of the ZMP. If the ZMP is located inside the support polygon¹ of the legged system, the system is considered to be dynamically stable. When the ZMP is located outside the support polygon, as indicated in figure 2.3, it is referred to as a fictitious zero moment point (FZMP) and can indicate that there is a disturbance in the system. [12] The distance between the edge of the foot and the FZMP can give an indication of how severe the disturbance is.

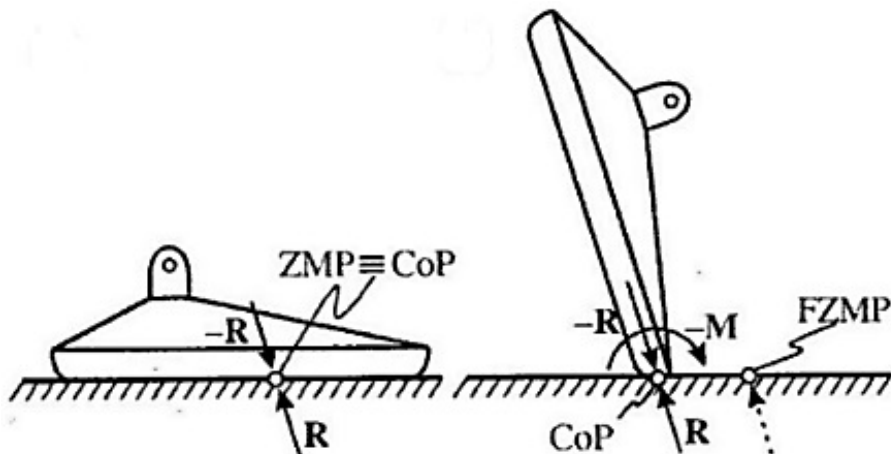


Figure 2.3: Zero Moment Point [13]

Rapid response motions are required to reject disturbances. These response motions can be divided into the following basic strategies [12]:

1. Ankle strategy - Ankles are used to apply torque forces that adjust ZMP position.
2. Hip strategy - Angular moments are created by bending the hips.
3. Stepping strategy - Biped steps forward to help absorb the disturbance force. This strategy is used when the ankle- and hip strategy are not sufficient.

¹A convex hull containing all the ground contacts of the legged system.

The simplest version of a walking robot is five-link bipedal robot [14]. The five-link model is limited to only the hip- and stepping-strategy because of the absence of ankles. When a robot encounters a disturbance force the ZMP shifts closer to the edge of the contact point, due to an increased moment around the contact point. The hip-strategy counters this by attempting to absorb the disturbance force and reduce the moment around the contact point. Resisting the disturbance force by holding the hips rigid or accelerating backwards has been proven [2] to increase the shift of the ZMP and leads to quicker instability of the robot. If a disturbance force is too large for the hip strategy to be effective, then the stepping strategy is required to compensate the disturbance. To apply the stepping strategy it is important to determine where the robot has to step to recover from the disturbance. A *capture point* is a point on the ground where the foot is placed to regain the stability of a legged system. [12] There can be infinite capture points and the area covering these points is called the *capture region*. [15] Figure 2.4 shows that considering the kinematic work space of the robot leg can assist in identifying whether the robot should take one or multiple steps to place the ZMP in the capture region.

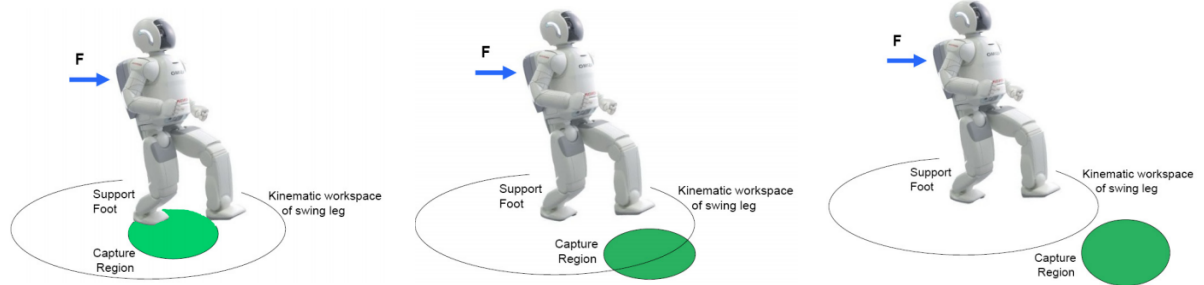


Figure 2.4: Capture Region [15]

Determining the capture regions for general humanoids is a very complex problem and biomedical studies [16] [17] have discovered a less complex solution that involves modelling a humanoid as a simple linear inverted pendulum. This model can then be used to approximate the capture region. The linear inverted pendulum is modelled by representing the body of the bipedal robot as a single mass, located at the robot's CoM, balancing on a stick that is attached to the feet of the robot. The exact closed form solutions of the capture region for the linear inverted pendulum model can be found in [15]. Further improvement of disturbance rejection can be done by adding features to a five-link robot that assist disturbance response motions. Possible features include adding arms, feet or even a tail. [18] [19] [20] As mentioned above in the disturbance response strategies, adding feet with ankles can be beneficial for the overall balance of a bipedal robot and can assist disturbance rejection. This statement is proven by results from [19] that show that the use of ankle joints can improve the energy efficiency of a robot's gait. The size of the feet can also affect the balance of the robot. Increasing the size of the feet increases the base of support(BoS) size which in turn improves the robots balance. [21]

Arms are a common feature found on humanoid robots as they can provide extra functionality to the robot. The Atlas robot indicated in figure 2.1 uses this extra functionality to operate power tools, open doors, pick up objects and execute many other tasks that bipeds without arms cannot perform. [22] Besides offering extra functionality, arms can also be used to apply a moment about the CoM of the robot to assist in disturbance rejection as proven in [23] [24]. The use of arm rotation strategies(ARS) for balance recovery of humanoids is tested in [24]. The approach used in [24] involved using Q-learning (reinforcement learning algorithm) to decide on optimal motions for a humanoid robot. Tests were then done to compare the balance of a humanoid with and without arms. These tests applied a variety of lateral impulse forces at the back of both models and the results recorded are given by figure 2.5. These results show that adding arms to a bipedal

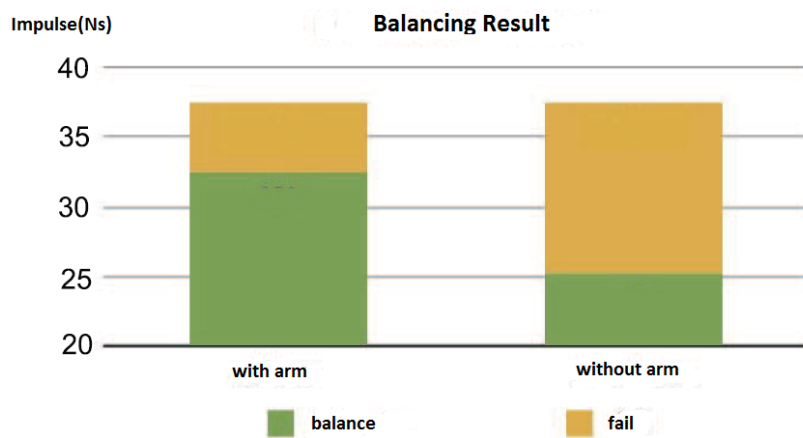


Figure 2.5: Arm rotation strategies(ARS) results from [18] Green represents a stable robot and yellow an unstable robot. The robot was considered unstable when the ZMP was located outside the BoS.

robot is not only beneficial for the functionality of the robot but can also assist the robot in disturbance rejection. It is also indicated in the study that the size of the moment that the arms can generate is dependent on the rate of the rotation, weight and length of the arm.

Most robotic tail designs to date have been used to balance quadrupedal robots and the use of a tail to balance a bipedal robot is a relatively unexplored idea. The concept of tails being used on robots is inspired by animals such as dinosaurs, kangaroos, lizards and multiple quadrupedal mammals. Besides improving the balance of the robot, tail designs can also offset some of the work done by the legs of the robot allowing for simpler mechanical leg designs. There are two main tail designs in robotics, namely the simple pendulum tail and the biomimetic multi-link tail. The multi-link tail is more complex solution but presents multiple advantages including generating higher inertia loadings. [20] Experiments done on the MIT cheetah [25] show that a biomimetic multi-link tail can be very effective with respect to disturbance rejection.

Chapter 3

Methodology

This chapter provides the design and execution plan used to address the two main goals of this study. These goals are determining whether trajectory optimisation can be used as a tool to help identify optimal disturbance rejection in bipedal robots and if adding arms to a five-link robot will improve its disturbance rejection. The methodology can be divided into five main aspects, namely the modelling of the bipedal robot, the optimisation model, the disturbance forces, the trajectory solver and analysis of the results.

3.1. Modelling

The two robot models indicated in figure 3.1 were used in this study to simulate results. The base model is a five-link bipedal robot and the second model is the same base model with a single-link arm added. These models were chosen because they are popular starting points in many robotic research studies. [6] [5] [14] The models consisted of rigid links that were connected via torque actuators and the dimensions of the models were based on the human dimensions [26] that were scaled down by half. The reason for this was so that comparisons could be made between humans and the models used in the simulation. The robot was scaled down to make the building of the bipedal robot more feasible, if practical tests were to be considered. The generalised coordinates for both models were as follows:

$$\mathbf{q}_{Biped} = [x, z, \theta_{Body}, \theta_{TibiaR}, \theta_{FemurR}, \theta_{TibiaL}, \theta_{FemurL}]$$

$$\mathbf{q}_{Biped+Arm} = [x, z, \theta_{Body}, \theta_{Arm}, \theta_{TibiaR}, \theta_{FemurR}, \theta_{TibiaL}, \theta_{FemurL}]$$

Due to these models having multiple degrees of freedom, determining the dynamics of them was a complex problem. It was therefore decided to use the Euler-Lagrange equations. Figure 3.1 shows that hips,knees and arm angles of the robot were defined as relative angles and the body angle of the robot was defined as an absolute angle between the z-axis and the body. While generating the EoM's the use of relative angles helped simplify the defining of the torques and forces applied to the general coordinates. The CoM positions of each link were also important for calculating the EoM's of the model. To calculate CoM positions the absolute angles were required and the these angles where determined

by calculating the difference between the applicable relative angles. The robot's CoM location was chosen to be at the base of the body.

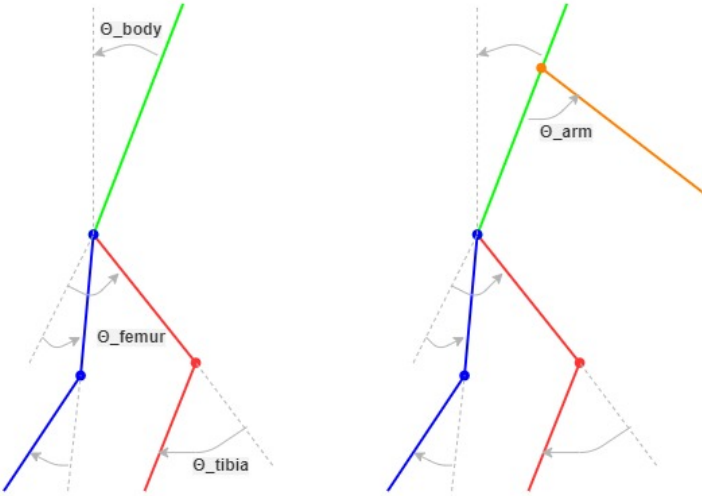


Figure 3.1: The two bipedal models simulated in this study are given above as well as the defined joint angles of the models.

3.2. Disturbance forces

The disturbance rejection of the model was tested by applying a variety of lateral forces at the mid-body and head of the robot. The disturbance forces were applied at the first node point and then set to zero for the rest of the node points (refer to figure 4.1). Due to the short time periods between nodes, a force applied on one node resembled an impact force. The magnitude of these forces were then gradually increased until the optimiser could not find a feasible solution. After each feasible solution was found, the solution data was stored for later analysis. For each new disturbance force tested, five solutions were stored to account for any outlier results.

3.3. Optimisation Model

To perform the trajectory optimisation it was important to first define the optimisation problem in Python code. This was done using Pyomo (Python Optimisation Modeling Object) software. The Pyomo software defines the optimization problem as an object-orientated model that is made up of a collection of modeling components. These modeling components are shown in figure 3.2 below. [27] The index set used for the Pyomo model was data that described the dynamics of the robot model. The dimensions of the bipedal robot, the gravity constant and moment of inertia values were the modeling parameters used in the Pyomo model. Decision variables were variables that the optimisation program altered in order to achieve the desired output. These variables are usually limited via

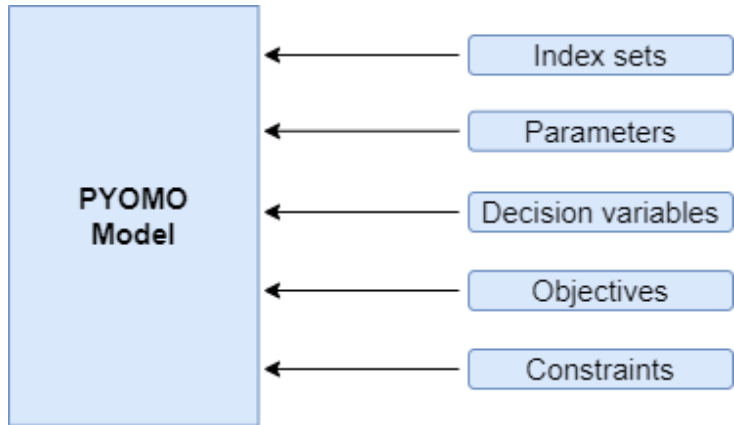


Figure 3.2: Modelling components of a Pyomo model

bounds or constraints. The focus of the trajectory optimisation was to minimise the energy consumption of the robot's motions and this was achieved by listing the torque actuation forces in the cost function, which is a type of objective function. The detailed design of the constraints and the other modeling components is provided in chapter 4.

3.4. Trajectory solver

IPOPT (Interior Point Optimiser) software was used to solve the non-linear optimisation problem that was defined with a Pyomo model. This process included generating a random seed (starting configuration of the model) and using the solver to test whether the seed would produce a feasible solution after the constraints, tolerances and desired objective function had been added. Due to the complexity of the problem there was the menace of the solver not always producing a feasible solution. In order to curb this issue techniques were applied to increase the probability of the solver finding a feasible solution. One of these techniques was to only randomise the initial values of the generalised coordinates during the seed generation and setting the values of the remaining variables to 0.01. The ϵ relaxation technique (regularisation method) was also applied to minimise time used to solve the complementarity constraints from the contact implicit optimisation method (refer to Chapter 4). The ϵ value was initially set to 1000 and the problem was solved iteratively four times with the ϵ value being reduced by a factor of 10 after each iteration was solved. When all four iterations were successfully completed the complementarity constraints were regarded as solved ($\alpha'(i)\beta'(i) = 0$, within the final tolerance of $\epsilon = 1$). [28] [29] If no feasible solution was found, the seed was rejected and a new randomised seed was initiated. Figure 3.3 provides a graphical presentation of the process followed by the trajectory solver.

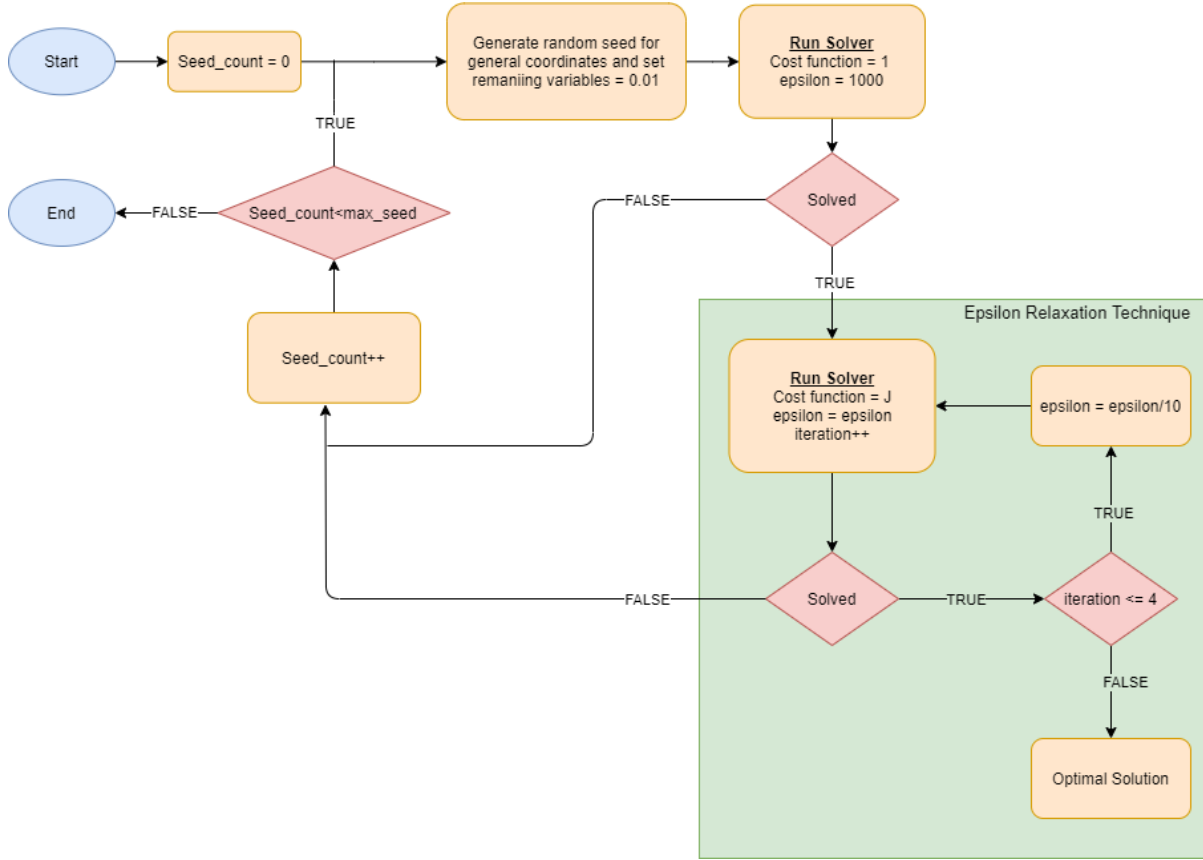


Figure 3.3: The above graphic provides an overview of the solver process and the green block indicates how the regularisation method was implemented.

3.5. Analysis

Analysis was done by examining two main aspects of the data collected. These were the ground reaction forces and the summed moments about the CoM. Focus was placed on comparing data from the simulations where the biped could reject a disturbance by only using the hip-strategy to data where the biped had to implement a stepping-strategy in addition to the hip-strategy to reject the disturbance. The goal of this was to be able to identify a criteria that describes when the biped needs to take a step forwards/backwards to reject a disturbance.

To simplify the analysis of the ground reaction force data, the data was presented in its polar coordinate values. The angles and magnitudes of the GRF data were then compared to help find the threshold values for the stepping strategy. Plotting the angle of the GRF at each node and the magnitude at each node assisted in determining trends. The angle of the GRF was calculated for each foot with following equation:

$$\theta_{GRF} = \arctan\left(\frac{GRF_z}{GRF_x}\right)$$

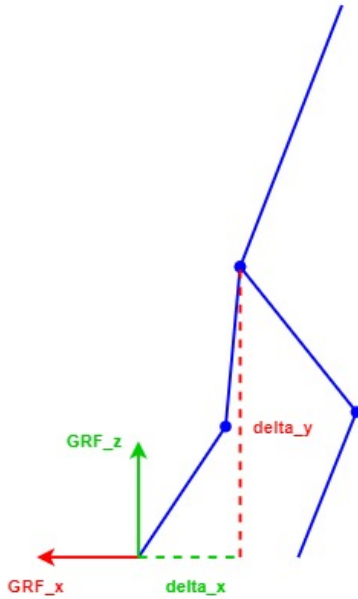


Figure 3.4: The GRF components used to calculate the moments about CoM

The moment about the CoM was calculated by multiplying the x - and z -components of the GRF with the correct distances (refer to figure 3.4) between the feet and CoM. The following equation was used to calculate the total moment:

$$m_{foot} = GRF_x \Delta_z + GRF_z \Delta_x$$

$$m_{total} = m_{rightfoot} + m_{leftfoot} + m_{disturbance}$$

where Δ_z and Δ_x where the x and z distances between the foot and CoM as indicated in figure 3.4. The moment created by the applied disturbance force was represented by $m_{disturbance}$. The m_{total} moments were calculated for each node point and then plotted for analysis.

Chapter 4

Trajectory Optimisation

Trajectory optimisation is a set of mathematical methods used to discover the optimal behaviour for a dynamical system. To reduce the size of the problem, bounds and constraints were added which the optimal trajectory had to satisfy. This chapter will provide a detailed description of trajectory optimisation and the design steps taken to implement it. Key topics covered in this chapter were the dynamics of the model, transcription and the direct-collocation trajectory optimisation, as well as the constraints and bounds of the system.

4.1. Euler-Lagrange dynamics

Calculating the EoM's of the bipedal robot models discussed in chapter 3 was done using Euler-lagrange dynamics. [30] Both models, as shown in figure 3.1, consist of inelastic links that are connected with torque actuator's. The CoM of each of these links were assumed to be in the centre of the link and the moment of inertia for each link was calculated by the following general equation.

$$I = \frac{1}{12}ML^2$$

The added arm for the second model was modelled as a point mass. This was done to make the arm more effective with disturbance rejection. The CoM of the arm was therefore located at the end of the arm link and the moment of inertia was calculated with the following equation:

$$I_{arm} = ML^2$$

where M is the mass of the specific link and L is the length of the link. To determine the EoM's it was important to first define the generalised coordinates(\mathbf{q}) and the applied torques(\mathbf{u}) which were as follows:

$$\mathbf{q}_{Biped} = [x, z, \theta_{body}, \mathbf{q}_{rightleg}, \mathbf{q}_{leftleg}]$$

$$\mathbf{q}_{Biped+Arm} = [x, z, \theta_{body}, \theta_{arm}, \mathbf{q}_{rightleg}, \mathbf{q}_{leftleg}]$$

$$\mathbf{q}_{leg} = [\theta_{femur}, \theta_{tibia}]$$

$$\mathbf{u}_{Biped} = [\mathbf{u}_{rightleg}, \mathbf{u}_{leftleg}]$$

$$\mathbf{u}_{Biped+Arm} = [\tau_{arm}, \mathbf{u}_{rightleg}, \mathbf{u}_{leftleg}]$$

$$\mathbf{u}_{leg} = [\tau_{hip}, \tau_{knee}]$$

The generalised coordinates were then used to calculate the position vector (P_{CoM}) of each link's CoM. The velocity vector was determined by calculating the Jacobian matrix of the position vector and multiplying the answer with the time derivative of the generalised coordinates.

$$\dot{P}_{CoM} = jacobian(P_{CoM}, \mathbf{q})\dot{\mathbf{q}}$$

Position and velocity vectors were used to calculate the potential and kinetic energy for each link of the robot. In the equations below T refers to kinetic energy, V is the potential energy, m is the mass of the respective link, g is the gravitational constant, ω is angular rate of the link and I is the moment of inertia of the link. The total kinetic and potential energy were calculated by summing the respective energies.

$$T = \frac{1}{2}m(\dot{P}_{CoM})^2$$

$$T_{rotational} = \frac{1}{2}I\omega^2$$

$$V = mg(P_{CoM})_z$$

Calculating the manipulator equation which is derived from Euler-Lagrange equations was the final step for determining the EoM's. [30] [28]

$$M(q, \dot{q})\ddot{q} = -C(q, \dot{q})\dot{q} + G(q) + Q(q) + A\lambda + B\delta$$

where M represents the mass matrix, C the Coriolis matrix and G the gravitational potential matrix. The torque forces that were applied to the specific general coordinates are represented with the Q matrix. The A and B matrices were used to map the external forces that were applied to the general coordinates of the system. The A matrix was multiplied by λ which represents the ground reaction forces as the following components:

$$\lambda = [\lambda_x, \lambda_z]^T$$

where λ_x is the horizontal component of the ground reaction forces and λ_z the vertical component. These components were calculated for each foot. The applied disturbance forces are represented by δ and were also divided into horizontal and vertical components.

$$\delta = [\delta_x, \delta_z]^T$$

To calculate the mass matrix M the following equation was used:

$$M(q, \dot{q}) = jacobian(jacobian(T_{total}, \dot{\mathbf{q}})^T, \dot{\mathbf{q}}))$$

where T_{total} represents the total kinetic energy. The Coriolis matrix gives the Coriolis and centrifugal force terms in the EoM and was calculated using following equation:

$$C(q, \dot{q}) = \frac{1}{2} \sum_{k=1}^N \left(\frac{\partial M_{ij}}{\partial \mathbf{q}_k} + \frac{\partial M_{ik}}{\partial \mathbf{q}_j} - \frac{\partial M_{kj}}{\partial \mathbf{q}_i} \right) \dot{\mathbf{q}}_k$$

The following pseudo code indicates how the above equation was implemented.

```

for i= 1:length(q)
for j= 1:length(q)
for k= 1:length(q)
hold = 0.5(diff(M[i,j],q[k]) + diff(M[i,k],q[j]) - diff(M[k,j],q[i]))q_k
C[i,j]= C[i,j] + hold
end
end
end

```

The G matrix that represents the effect of the gravitational forces on the model was calculated from the equation below.

$$G(\mathbf{q}) = \frac{\partial V_{total}}{\partial \mathbf{q}}$$

where V_{total} is the total potential energy of the system. The pseudo code used for this equation is:

```

for n= 1:length(q)
G[n]= diff( $V_{total}$ ,q[n])
end

```

The A matrix maps the ground reaction forces to the general coordinates of the system and it was calculated by the following equation:

$$A = jacobian(P_{foot}, \mathbf{q})^T$$

where P_{foot} is the position of the foot. The calculation was done for each foot. The applied torque forces are presented in the Q matrix, which is defined as follows:

$$Q_{biped}(\mathbf{q}) = \begin{bmatrix} 0 \\ 0 \\ \tau_{body} \\ -\tau_{knee'R} \\ \tau_{hip'R} \\ -\tau_{knee'L} \\ \tau_{hip'L} \end{bmatrix}$$

The Q matrix for the biped with the added arm included an additional entry for the torque force applied to the arm. This hard coded approach was possible due to the use of relative angles in the defining of the general coordinates. Lastly, the B matrix was calculated. The B matrix is similar to the A matrix and was used to map the applied disturbance forces to the general coordinates. The B matrix was calculated using the following equation:

$$B = jacobian(P_{disturbance}, \mathbf{q})^T$$

where $P_{disturbance}$ is the position of the disturbance.

4.2. Transcription

When performing trajectory optimisation the initial problem is usually defined with the following general equation:

$$\min_{t0, tf, x(t), u(t)} J(t0, tf, x(t0), x(tf)) + \int_{t0}^{tf} \omega(\tau, x(\tau), u(\tau)) d\tau$$

where J is the boundary objective and ω is the path integral along the trajectory. Transcription is a crucial step in trajectory optimisation and it is the process of converting the above-mentioned initial trajectory optimisation problem into a constrained parameter optimization problem (non-linear program). The main differences between the trajectory optimisation problem and the constrained parameter optimization problem are as follows:

1. The decision variables for the trajectory optimisation problem are infinite dimensional vector functions whereas the the decision variables for a constrained parameter optimization problem are real numbers of finite dimensionality.
2. The trajectory optimisation problem uses differential equations whereas the constrained parameter optimization problem uses only algebraic equations.

Because of these differences, converting the problem to a constrained parameter optimisation problem will make it easier to solve. There is a large variety of transcription processes and this study focused on the direct-collocation method as it is a popular method used with robotics. [31]

4.3. Direct-collocation Method

The direct-collocation method converts the continuous trajectory optimisation problem into a discrete problem by approximating all the continuous functions in the problem statement as a sequence of polynomial sections. It is important to note that the direct method discretises the optimisation problem before it is optimised whereas other transcription methods discretise after optimisation. This makes the direct method easier to present and solve compared to other methods. The actual discretisation is done using the collocation method. Before the collocation can be implemented the decision variables of the system have to be defined. [31] [28]

The decision variables are the variables that the optimisation program adjusts to achieve the desired solution. The decision variables for this study were as follows:

$$x = [\mathbf{q}(i, j), \dot{\mathbf{q}}(i, j), \ddot{\mathbf{q}}(i, j), \mathbf{q}_0(i), \dot{\mathbf{q}}_0(i), \ddot{\mathbf{q}}_0(i), \tau(i), \mathbf{h}(i), \mathbf{tt}(i, j), \mathbf{tt}_0(i), \lambda(i, j), \mathbf{slack}(i, j)]$$

The EoM's of the system are the source of the $\mathbf{q}(i, j)$, $\dot{\mathbf{q}}(i, j)$, $\ddot{\mathbf{q}}(i, j)$, $\tau(i)$ and $\lambda(i, j)$ decision variables. The difference between $\mathbf{q}(i, j)$ and $\mathbf{q}_0(i)$ and their time derivatives is that $\mathbf{q}(i, j)$ considers the values at the collocation points(j) and at the node points(i) whereas $\mathbf{q}_0(i)$ only considers the values at the node points(i) (refer to figure 4.1). The $\mathbf{h}(i)$ variable represents the time intervals between nodes and the $\mathbf{slack}(i, j)$ variable is used with the implementation of the complementarity constraints. The $\mathbf{tt}(i, j)$ is total time up to the i_{th} node point and j_{th} collocation point. The $\mathbf{tt}_0(i)$ variable is the same as the $\mathbf{tt}(i, j)$ variable, but only considers the node points when determining the total time.

4.3.1. Collocation

Collocation is an approximation function that is used in conjunction with the direct method and is responsible for how accurately each of the polynomial sections represent the continuous function. The collocation process first takes the continuous general coordinates and discretises them into N nodes. The higher the N value, the longer the solver will take to find a solution. For this study N varied between 30 and 60. Determining the trajectory between nodes (polynomial sections) was done using three collocation points that were calculated using the three-point Radau method using the coefficients in the Butcher tableau from Runge Kutta. The Radau method is specifically used to solve the

equations of motions at chosen time points with an accuracy of h^{2K-1} where h is time-step and K is number of collocation points. [31] [28] [29] The equations used to perform the three-point Radau method were as follows:

$$\mathbf{q}(i, j) = \mathbf{q}_0(i) + h(i) * \sum_{k=1}^3 a(k, j) \dot{\mathbf{q}}(i, k)$$

$$\dot{\mathbf{q}}(i, j) = \dot{\mathbf{q}}_0(i) + h(i) * \sum_{k=1}^3 a(k, j) \ddot{\mathbf{q}}(i, k)$$

$$a = \begin{bmatrix} 0.19681547722366 & 0.39442431473909 & 0.37640306270047 \\ -0.06553542585020 & 0.29207341166523 & 0.51248582618842 \\ 0.02377097434822 & -0.04154875212600 & 0.11111111111111 \end{bmatrix}$$

where a is the collocation matrix that was used to help approximate the positions of the collocation points. To guarantee a continuous state trajectory the $\mathbf{q}(i, 3)$ values and $\mathbf{q}_0(i+1)$ values have to be equal as indicated in figure 4.1. The following equations were implemented to ensure this:

$$\mathbf{q}_0(i) = \mathbf{q}(i-1, 3)$$

$$\dot{\mathbf{q}}_0(i) = \dot{\mathbf{q}}(i-1, 3)$$

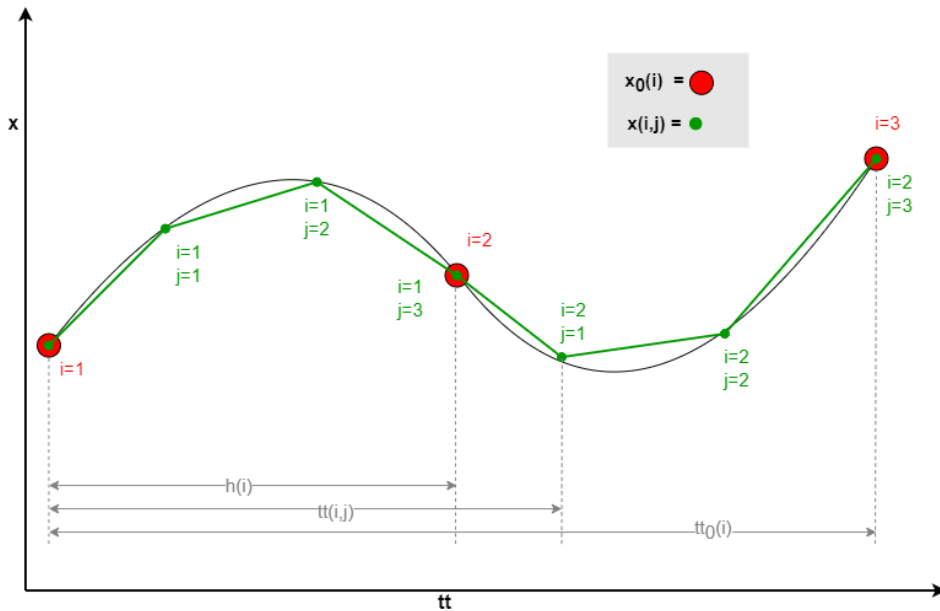


Figure 4.1: The graph above indicates how the collocation method discretises the continuous functions into node(i) and collocation(j) points. The red dots represent node points and the green dots the collocation points. The $h(i), tt(i, j)$ and $tt_0(i)$ decision variables are also presented in the graph.

The contact points for the model were required to occur on the node points and therefore a time period variable was used to offer leniency to the time step between nodes. Before the time variables could be calculated the following constraint was added:

$$hm = \frac{T}{N}$$

$$0.5hm \leq h(i) \leq 2hm$$

where T is a scaling factor used to alter the time steps and N is total number of nodes. The constraint sets a boundary for a minimum and maximum time step. The time variables were then calculated with the following equations:

$$\mathbf{tt}(i, j) = \mathbf{tt}_0(i) + h(i) * \sum_{k=1}^3 a(k, j)$$

$$\mathbf{tt}_0(i) = \mathbf{tt}(i - 1, 3)$$

As indicated in figure 4.1 the $h(i)$ variable is the time step between nodes and $tt(i, j)$ is the total time from the start up to a specific collocation point. The $tt_0(i)$ is the total time up to a specific node point.

4.4. Constraints and bounds

Once the trajectory optimisation problem has been converted to a non-linear program using transcription the bounds and constraints can be added via basic algebraic equations. Adding bounds and constraints helps model the optimisation problem and allows the solver to find a solution quicker as it reduces the search space.

4.4.1. General coordinates

Constraints were added to the general coordinates of the robot to limit the motions and velocities of the coordinates to a more realistic range. The constraints added were as follows:

Constraints for x and z coordinates [m and m/s]:

$$-\frac{3}{2} < \mathbf{x} < \frac{3}{2}$$

$$0 < \mathbf{z} < \frac{3}{2}$$

$$-10 < \dot{\mathbf{x}} < 10$$

$$-10 < \dot{\mathbf{z}} < 10$$

Constraints for joint angles [rad and rad/s]:

$$-\frac{\pi}{2} < \theta_{Body} < \frac{\pi}{2}$$

$$-\pi < \theta_{Arm} < \pi$$

$$-\frac{\pi}{2} < \theta_{Hip} < \frac{\pi}{2}$$

$$0 < \theta_{Knee} < \frac{5\pi}{9}$$

$$-\omega_{max} < \dot{\theta}_{Body} < \omega_{max}$$

$$-\omega_{max} < \dot{\theta}_{Arm} < \omega_{max}$$

$$-\omega_{max} < \dot{\theta}_{Hip} < \omega_{max}$$

$$-\omega_{max} < \dot{\theta}_{Knee} < \omega_{max}$$

where $\omega_{max} = 44\text{rad/s}$. These constraints were chosen as very lenient ranges for the robot to adhere to and still gave the trajectory optimiser the freedom to independently identify the optimal motion for the robot.

4.4.2. Motor model

A motor model was created to restrict the torque actuators so that the study results would be more relevant to robotic platforms. When applying these constraints the stall torque(τ_{max}), no load speed(ω_{max}) and the angular velocity($\omega(i)$) of the specific joint were considered. The constraints were implemented as follows:

$$-\tau_{max} - \frac{\tau_{max}}{\omega_{max}}\omega(i) < \tau(i) < \tau_{max} - \frac{\tau_{max}}{\omega_{max}}\omega(i)$$

where:

$$\tau_{max} = 12\text{Nm}$$

$$\omega_{max} = 44\text{rad/s}$$

The max values of the torque actuators were based on a T-motor A80-6 torque actuator. Even though this torque actuator was relatively weak for the size of the robot model being simulated it still produced sufficient torque for the robot to perform the disturbance rejection motions. [28] [29]

4.4.3. Contact Implicit Method

One of the main focus points of this study was to use trajectory optimisation as a tool to determine the optimal motions of a bipedal robot. In order to achieve this, the contact order of the robot's gait could not be enforced and the trajectory optimiser had to determine the contact order independently using the contact implicit optimisation method. The disadvantage of this method is the large amount of complementarity constraints needed to ensure that the ground reaction forces are only applied when the feet are in contact with the floor. [28] [29] The method was implemented by dividing the ground reaction forces for each foot into the following components:

$$\lambda_{GRF} = [\lambda_x^+ - \lambda_x^-, \lambda_z]$$

Given that:

$$\lambda_x^+, \lambda_x^-, \lambda_z \geq 0$$

The following complementarity constraint was implemented for each foot to ensure the ground reaction forces were only applied when the foot was in contact with the floor:

$$\phi(\mathbf{q})\lambda_z = 0$$

The $\phi(\mathbf{q})$ represents the height of the foot and therefore only when the height is zero and the foot is in contact with the floor will the constraint be satisfied. The friction and slipping factors also had to be considered when the foot is in contact with the floor. A friction cone was applied with the following constraint:

$$\mu\lambda_z - \lambda_x^+ - \lambda_x^- \geq 0$$

where μ is the friction coefficient ($\mu = 1$ was chosen). To ensure that the friction occurred within the friction cone when the foot slid the following complementarity constraint was added:

$$(\mu\lambda_z - \lambda_x^+ - \lambda_x^-)^T \gamma = 0$$

where γ represents the magnitude of the relative velocity. The magnitude of relative tangential velocity $\Psi(\mathbf{q}, \dot{\mathbf{q}})$ had to be calculated to implement the final constraint for a sliding foot. The magnitude of relative tangential velocity $\Psi(\mathbf{q}, \dot{\mathbf{q}})$ was calculated with the following constraints:

$$\gamma + \Psi(\mathbf{q}, \dot{\mathbf{q}}) \geq 0$$

$$\gamma - \Psi(\mathbf{q}, \dot{\mathbf{q}}) \geq 0$$

Given that:

$$\gamma \geq 0$$

Lastly, the two complementarity constraints below were added to ensure the horizontal ground reaction forces acted against the sliding motion of the foot:

$$(\gamma + \Psi(\mathbf{q}, \dot{\mathbf{q}}))\lambda_x^+ = 0$$

$$(\gamma - \Psi(\mathbf{q}, \dot{\mathbf{q}}))\lambda_x^- = 0$$

Due to the complexity of these complementarity constraints a regularisation method was applied to assist the solving of the foot contacts. The method was implemented by dividing the complementarity constraints into two parts, namely α and β . The complementarity constraints could then be expressed as the following:

$$\alpha\beta < \epsilon$$

where ϵ is the relaxation factor of the regularisation method. This method solved the complementarity constraints iteratively to within an acceptable tolerance by starting with a high tolerance and reducing the tolerance with each iteration ($\epsilon=1$ was chosen for the final iteration). The equation above was simplified even further by summing the complementarity constraints across the collocation points(j) and only assessing them at each node(i). This changed the above-mentioned equation to the following:

$$\alpha'(i)\beta'(i) < \epsilon$$

$$\alpha'(i) = \sum_{j=0}^K \alpha(i, j)$$

$$\beta'(i) = \sum_{j=0}^K \beta(i, j)$$

4.4.4. Terminal conditions

Terminal conditions are conditions that describe the end configuration of the simulation. These conditions can vary depending on the desired task of the biped. The task of the biped in this study was to successfully implement a disturbance rejection motion and then return to its original posture. The recovery of the original posture was implemented with the following constraints:

$$\mathbf{q}_0(i) = \mathbf{q}_0(1)$$

$$\dot{\mathbf{q}}_0(i) = \dot{\mathbf{q}}_0(1)$$

Chapter 5

Results and Analysis

Type	Magnitude	Applied at node(s) N	Location	Number of samples collected
Lateral push	$500N$	1	mid-body back	5
Lateral push	$1000N$	1	mid-body back	5
Lateral push	$1500N$	1	mid-body back	5
Lateral push	$2000N$	1	mid-body back	5
Lateral push	$400N$	1	mid-body front	5
Lateral push	$500N$	1	mid-body front	5
Lateral push	$600N$	1	mid-body front	5
Lateral push	$300N$	1	head back	5
Lateral push	$500N$	1	head back	5
Lateral push	$300N$	1	head front	5
Lateral push	$500N$	1	head front	5

Table 5.1: Disturbance tests simulated on the five-link biped model

Table 5.1 above shows the test data that was collected from the trajectory optimisation simulations. Note that all disturbance forces were only applied at node one and the time period of the disturbance forces were dependent on the time interval between the first and second node. The time intervals between nodes were described by the following equation and constraint:

$$hm = \frac{T}{N}$$

$$0.5hm \leq h(i) \leq 2hm$$

where $T = 0.5$ and $N = 30$. Therefore, the time periods of the applied disturbance forces were:

$$0.0083s \leq t_{disturbance} \leq 0.0333s$$

The small $t_{disturbance}$ values allowed for the larger magnitude values seen in table 5.1. To justify these magnitudes, the disturbance forces were calculated as impulse forces($magnitude * time$) and compared to the impulse forces used in other studies (refer to table 2.1). It is also important to note that when the front disturbances were simulated the biped was facing the opposite direction to when the back disturbances were simulated.

This meant that when comparing the disturbances applied at the back to the disturbances applied to the front of the biped the results from the front disturbances had to be reversed. From the analysis it was also noted that for some of the simulations the ground reaction forces were still acting on the foot while the foot was raised above the ground. This is due to the ϵ value from the regularisation method being too big and for future studies it is suggested that a smaller ϵ is chosen, for example $\epsilon = 10^{-4}$. The chosen $\epsilon = 1$ was, however, small enough to ensure that ground reaction forces acting on the raised foot were too small to have effect on the results.

5.1. Mid-body disturbances

For the mid-body forces applied at the back, the animations of simulated results shown by figures C.1 and C.2 indicated that the biped could not reject the 1500N and 2000N disturbance forces without stepping forwards. The simulated results also indicated that the biped successfully rejected one out of the five seeds simulated with the 1000N disturbance without using the stepping strategy. This could suggest that the 1000N disturbance was the limit at which it was still possible for the robot to reject the disturbance without stepping. For the 500N force the biped rejected the disturbance by lifting one leg slightly for a short period and implementing the hip-strategy. Using the information gained from viewing the animations further analysis was done by viewing the angles of the respective ground reaction forces plotted in the figures 5.1, C.9 and C.10. When investigating the nodes close to where the disturbance force was applied a trend was noticed with regards to the angle of the ground reaction forces. The GRF angles of both feet at the first node, for tests where the biped took a step to reject the disturbance, were almost always equal to -45 degrees. Further analysis of the GRF angles also indicated that the angles at the other nodes varied in the ranges of -45 to -90 degrees and +45 to +90 degrees. The reason for the varying angles was the biped attempting to balance itself by trying to relocate its ZMP to directly below its feet. By viewing the simulated biped step with the GRF forces added as seen in figure 5.2, further analysis of the GRF angles and the disturbance response motion could be done. Figure 5.2 revealed that the 2000N force applied at node one for seed=1 caused the GRF angles of both feet to start at -45 degrees. This implies that at node one the ZMP had already started shifting over the front edge of the foot. The biped then rapidly attempted to counter the moment created by the disturbance force by shifting the GRF angle of the one foot to +45 degrees at node three. It did this by leaning back slightly and bending the knees to help shift the CoM and also help absorb the disturbance. The figure showed that this attempt was not successful and the biped eventually had to step forwards. The magnitude of the moments created by these ground reaction forces were also investigated and shown in figure 5.3. When examining the graph with the moments of all the seeds it can be seen that the majority of the moments on

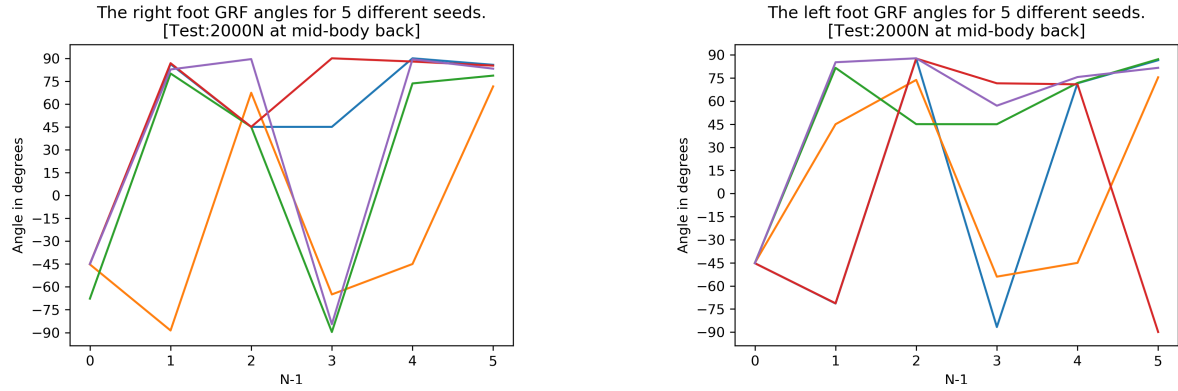


Figure 5.1: The ground reaction force angles of the right and left foot when 2000N lateral force is applied at the back of mid-body for five different seeds. Only the first six nodes are shown to make the graph more comprehensible.

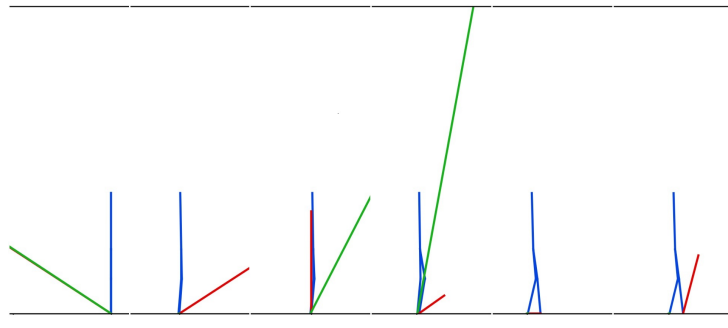


Figure 5.2: 2000N lateral force applied at back of mid-body - This figure considers the data from a single seed (seed=1) and shows the GRF forces applied to the feet for nodes [1,3,6,9,11,13]. Green represents the left foot's GRF forces and red the right foot's GRF forces. (Note: The magnitudes of the GRF forces were shortened when creating this figure and therefore can not be viewed as accurate.)

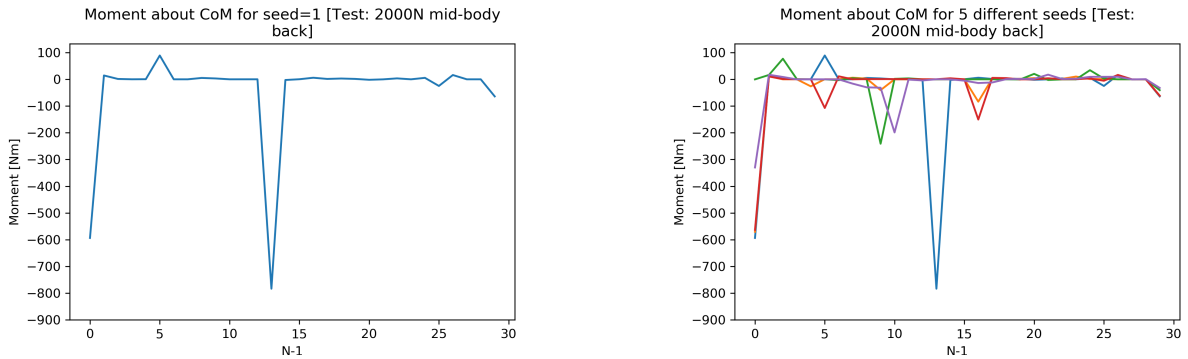


Figure 5.3: 2000N lateral force applied at back of mid-body - These figures show the total moment about the CoM of the biped for each node. The left figure is the moments for a single seed(seed=1) and the right figure shows the moments of all five different seeds simulated.

the first node are between -330 Nm and -594 Nm. The moments for the simulated biped step in figure 5.2 are also given on a separate graph in figure 5.3. Figure C.1 shows that

for this specific seed (seed=1) the biped had to take two full steps to recover from the disturbance whereas the other seeds only required one full step accompanied by smaller step to recover posture. This explains the large spike in the moment about the CoM at the start of node 13. As shown in figure 5.2, node 13 is where the biped completes its first step and the data from figure 5.3 suggests that the biped still had momentum and required a second step to reduce this momentum. This specific seed being analysed also had the largest moment ($M = -594Nm$) at node 1, which led to the capture region being located on the outside of the kinematic work space and forcing the biped to take two full steps to recover from the disturbance.

The simulations proved that the biped did not need to step forwards when the 500N disturbance was applied at the back of the body. Therefore, analysing the data from the 500N force was important to help build a criteria that would indicate when the stepping strategy was not required. The typical motion used by the biped to reject this disturbance was to bend the body slightly backwards and forwards and to lift the one leg for a period of time before returning it to its original position. This motion is also shown in figure C.4. When examining the GRF angles in figure 5.4 it can be seen that the angles at node one are all equal to +90 degrees. If the GRF angle is equal to ± 90 degrees it means the that the ZMP is located directly below the foot and the system can be considered dynamically stable. However, after node one the GRF angles varied in the same range as identified in the analysis of the other mid-body disturbance results. Figure 5.5 shows the simulated motion of seed=2 with its added GRF forces. The figure

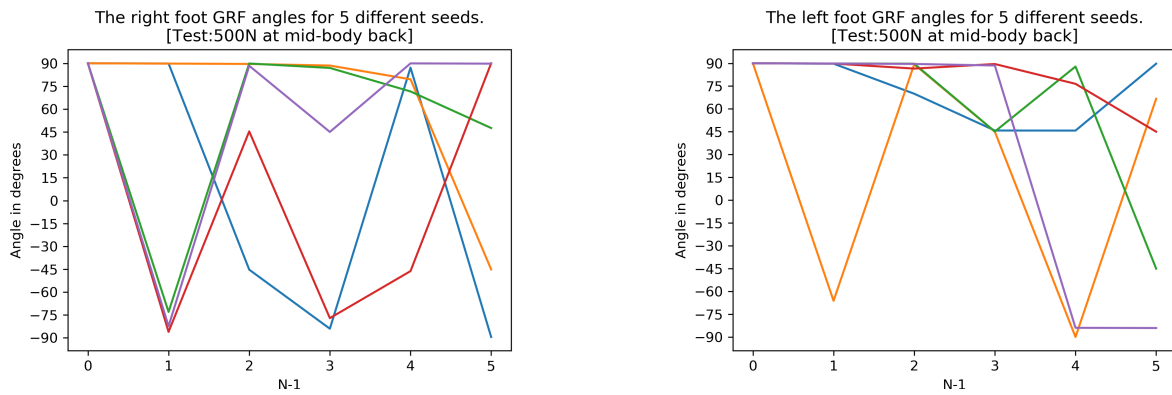


Figure 5.4: The ground reaction force angles of the right and left foot when 500N lateral force is applied at the back of mid-body for five different seeds. Only the first six nodes are shown to make the graph more comprehensible.

indicates that at node two the GRF angle of the left foot had already shifted to -66 degree angle causing a small clockwise moment about the CoM. This moment can be seen in the graph on the left in figure 5.6. This is due to the 500N disturbance pushing the CoM forward which leads to the ZMP shifting towards the front edge of the foot. Once the ZMP reaches the edge of the foot the GRF angle starts to decrease. At nodes 3,4, and 5

the biped attempts to reject the disturbance by leaning back with the body to create a counter-moment. The counter-moment creates an oscillation in the biped's movement as it tries to balance backwards and forwards using the hip strategy. This can be seen by the GRF angles in figure 5.4 jumping between the positive and negative values. Due to the fluctuations of the GRF angles, the moments about CoM reached a peak of $-45.1Nm$ at node 6. At node 7 the biped started lifting its leg to help shift the CoM forward while it leaned back with its body to counter the $-45.1Nm$ moment. This technique proved to be very effective in absorbing the peak moment and restoring balance to the robot as indicated in figure 5.5 and 5.6.

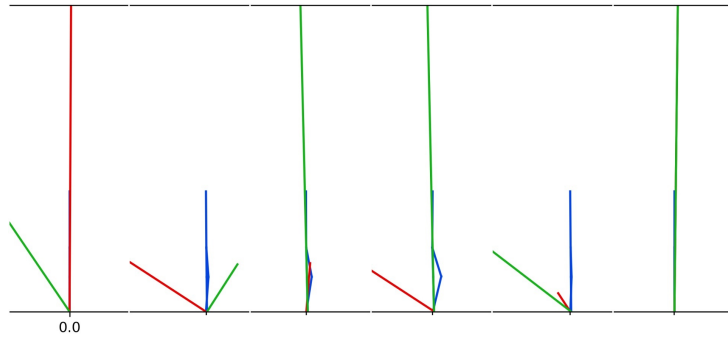


Figure 5.5: 500N lateral force applied at back of mid-body - This figure considers the data from a single seed (seed=2) and shows the GRF forces applied to the feet for nodes [2,6,12,18,24,30]. Green represents the left foot's GRF forces and red the right foot's GRF forces. (Note: The magnitudes of the GRF forces were shortened when creating this figure and therefore can not be viewed as accurate.)

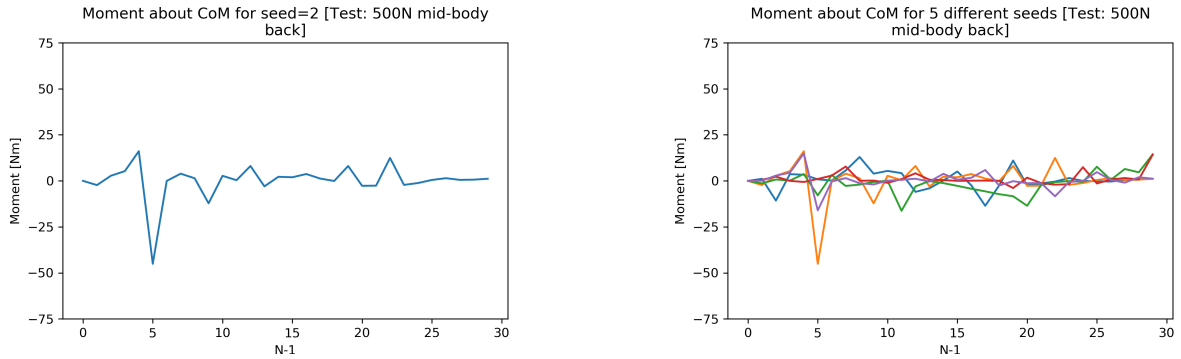


Figure 5.6: These figures show the total moment created by the GRF forces about the CoM of the biped for each node. The left figure is the moments for a single seed(seed=2) and the right figure shows the moments for all the seeds.

The three disturbance forces applied to the front of the mid-body were lateral forces with the magnitudes of 400N, 500N and 600N. Simulations of the 400N, 500N and 600N forces showed that the typical motion used by the biped to reject these disturbances

included the bending of the body and knees to help absorb the disturbance and taking at least one step backwards. This rejection motion can be seen in figure C.6. The motions used to reject the 400N disturbance were less consistent and only three out of the five seeds used the motion described above. The motions simulated from the other two seeds included the biped jumping back with both feet or the biped sliding its one leg back while bending the knees and body. The 600N test also produced slightly different motions for two of its seeds that required two steps backwards instead of one to recover. Examination of the GRF angles in figure 5.7 indicated that the angles on the node where the disturbance force was applied ($N=1$) are similar to those in the other mid-body disturbance tests. The only difference was that instead of both feet starting on -45 degrees, the one foot varied between -45 degrees and -70 degrees. This suggested that for some of the seeds simulated the ZMP had started shifting over the edge of the right foot before the left foot causing the right foot's GRF angle to reach -45 degrees earlier. This was due to the feet positions not being exactly the same and the disturbance force not shifting the ZMP as rapidly as the other disturbance tests. Further analysis was done

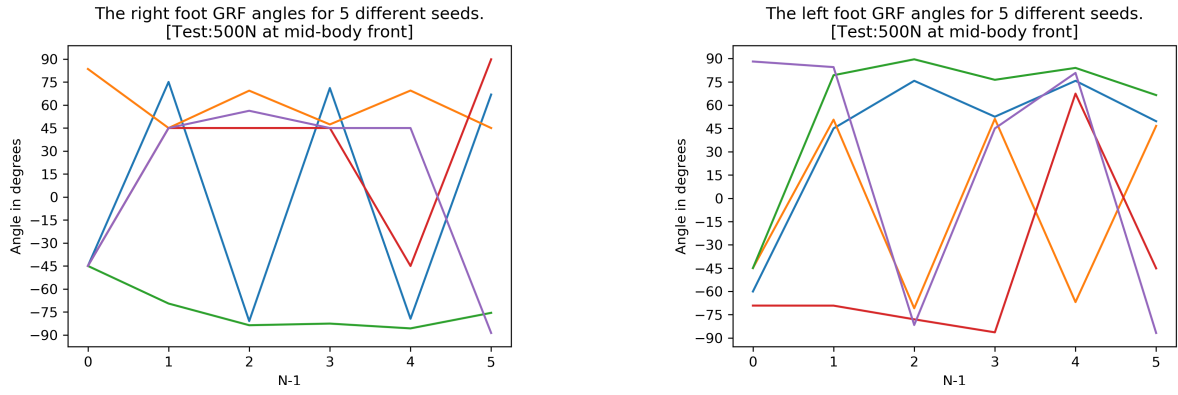


Figure 5.7: The GRF angles of the right and left foot for the first six nodes. The disturbance was a 500N lateral force is applied at the front of the mid-body.

by comparing the simulated motion of one of the seeds(seed=4) with its moments. Figures 5.8 and 5.9 showed that the initial disturbance created a small clockwise moment that the robot successfully absorbed by node seven by bending its knees and body. The biped tried to recover its original posture at node 18 which caused a large counter clockwise moment. The biped rejected this moment by stepping backwards with one leg. By examining figures 5.9 and C.12, that describe the moments about the CoM for other similar disturbances, it was determined that the moments showed no uniqueness with respect to what response strategy was used. Therefore, a mid-body disturbance response criteria could not be identified with the use of the moments about the CoM. This could be due to the disturbances being applied directly to the CoM which led to the disturbances not being properly conveyed in the moments about the CoM graphs. A better approach to analyse the mid-body disturbance could be to examine the position of the CoM with respect to the feet.

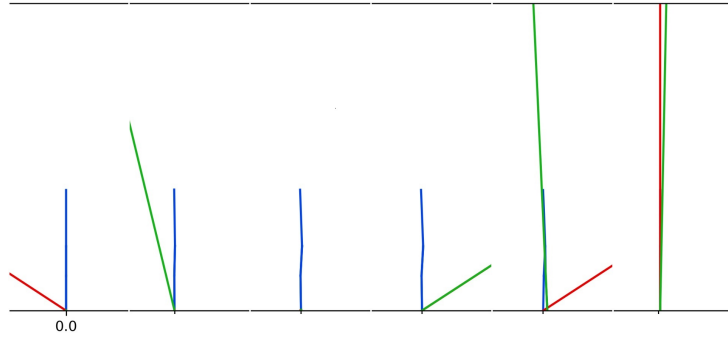


Figure 5.8: 500N lateral force applied at the front of the mid-body - This figure considers the data from a single seed (seed=4) and shows the GRF forces applied to the feet for nodes [1,7,17,19,24,30]. Green represents the left foot's GRF forces and red the right foot's GRF forces. (Note: The magnitudes of the GRF forces were shortened when creating this figure and therefore can not be viewed as accurate.)

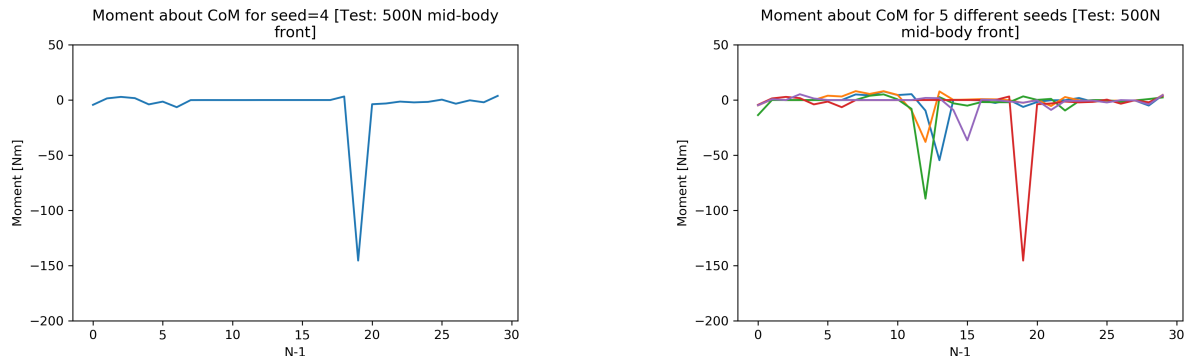


Figure 5.9: These figures show the total moment created by the GRF forces about the CoM of the biped for each node. The left figure is the moments for a single seed(seed=4) and the right figure shows the moments for all the seeds.

5.2. Head disturbances

The head disturbances were implemented with a lateral force that was applied at the top point of the biped's body link. The typical rejection motion simulated for the biped, when the 500N force was applied at the back the head, included the biped leaning forward with the body to help absorb the disturbance while bending the knees to help shift the CoM backwards. In addition to this motion the biped took a step forward to fully recover from the disturbance. For the 300N disturbance the biped used a similar motion but instead of stepping forward the one leg of the biped slid back a small distance. The majority of the GRF angles in figure 5.10 at the first node ranged from +45 degrees to +90 degrees. This implies that the moment created by the disturbance at node one shifted the ZMP towards the back edge of the foot. Figure 5.10 also shows that the GRF angles of the rest of the

nodes fluctuated in the following range:

$$-45^\circ \geq \theta_{GRF} \geq 45^\circ$$

This is the same range that was noted in the mid-body tests. Using the same analysis approach as in the previous tests, the simulated motion of the biped, as well as the moments about the CoM, were considered. When calculating the moments about the CoM for the head disturbance results it was important to include the moment created by the disturbance itself and not just the moments created by the ground reaction forces. Examination of figures 5.11 and 5.12 showed that the disturbance applied at node one

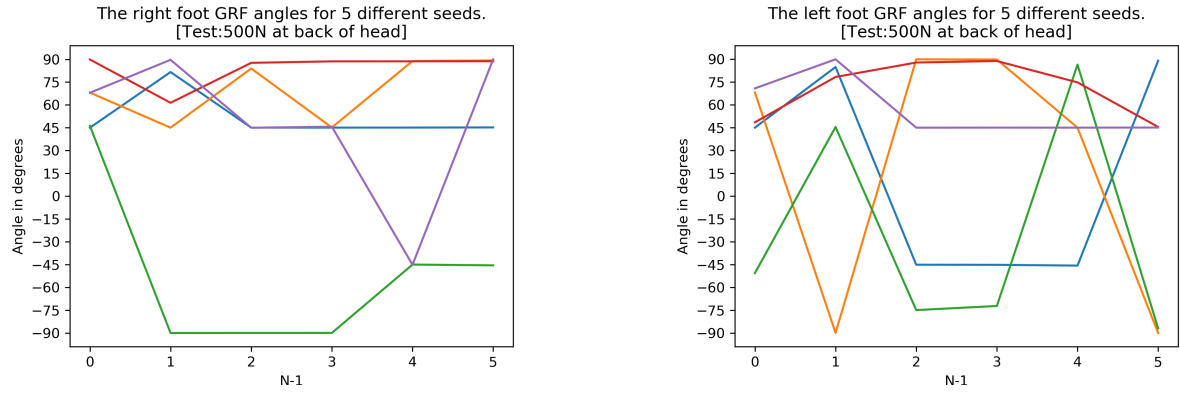


Figure 5.10: Ground reaction force angles of the right and left foot for the first six nodes when 500N lateral force is applied at the back of head

caused a large clockwise moment that the biped initially attempted to counter through rapidly shifting the ZMP over the back edge of both feet. This led to the GRF angles of both feet to start at +45 degrees as shown in figure 5.11. The biped shifted the ZMP to the back of the foot by leaning backwards and essentially shifting its CoM backwards. To avoid falling backwards from this motion the biped bent its knees and leaned forward with its body. This helped relocate the CoM back to above the feet in a more controlled manner and reduced the fluctuation of the moments about the CoM. The opposite GRF angles seen at node eight in figure 5.11 were caused by the falling back motion of the biped coupled with the rapid leaning forward of the body. The magnitude of the right foot's ground reaction forces at node eight was much larger than that of the left foot, which explains the spike in the moment about the CoM in figure 5.12. To reject this spike the biped had to bend its knees further to shift the CoM in the negative x-direction. When the biped attempted to recover its original posture at node 15 it was forced to take a step forwards. However, when viewing the moments about the CoM it could be seen that there were no large moments that motivated this step. This suggests that the trajectory optimiser identified the stepping strategy as the optimal approach to restore the posture of the biped.

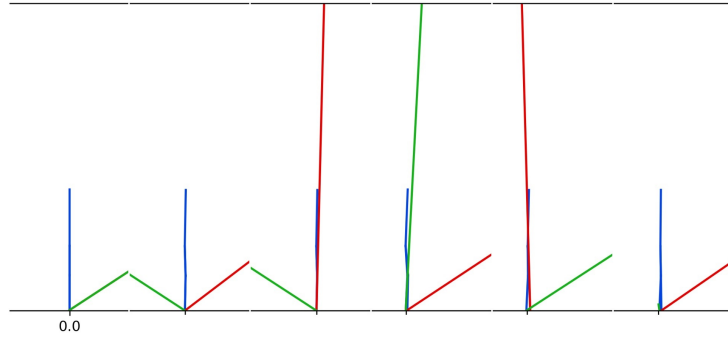


Figure 5.11: 500N lateral force applied at the back of the head - This figure considers the data from a single seed (seed=1) and shows the GRF forces applied to the feet for nodes [1,8,9,15,19,25]. Green represents the left foot's GRF forces and red the right foot's GRF forces. (Note: The magnitudes of the GRF forces were shortened when creating this figure and therefore can not be viewed as accurate.)

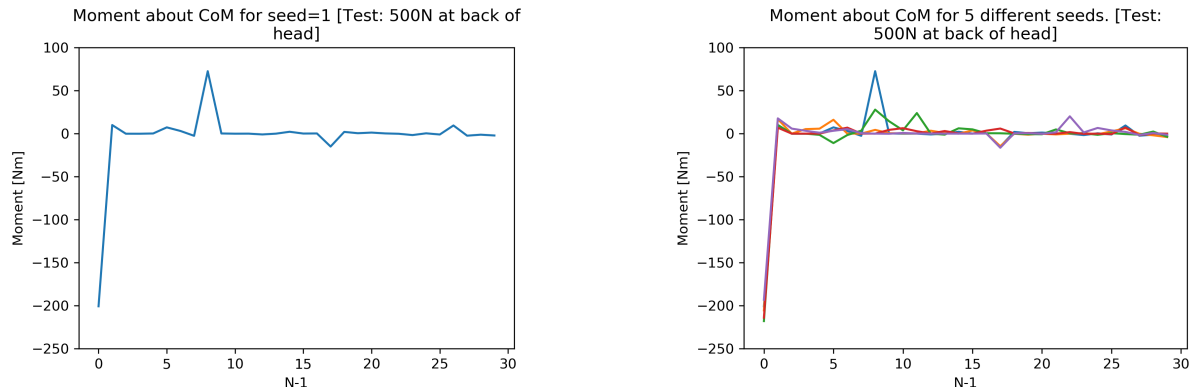


Figure 5.12: These figures show the total moment created by the GRF forces about the CoM of the biped over all 30 nodes. The left figure is the moments for a single seed(seed=1) and the right figure shows the moments for all the seeds.

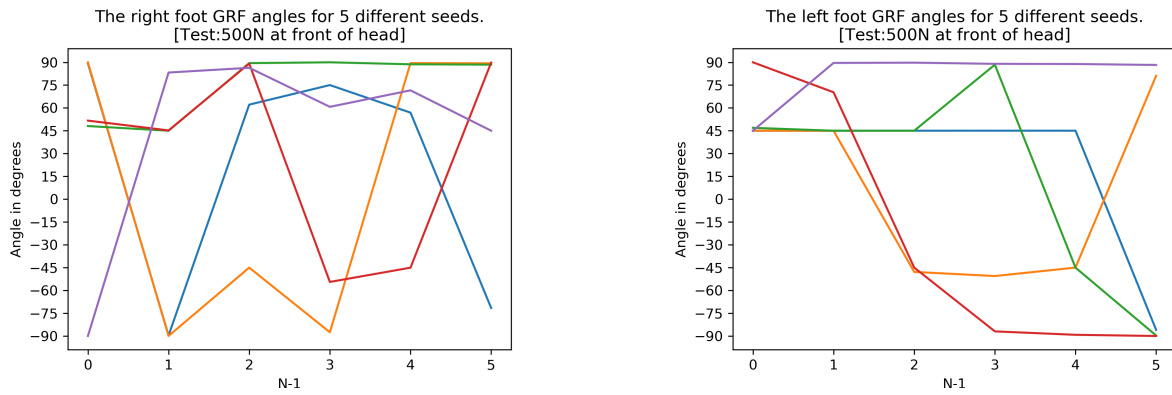


Figure 5.13: Ground reaction force angles of the right and left foot for the first six nodes when 500N lateral force is applied at the front of head

The animation shown by figure C.7 indicates the typical disturbance rejection motion when a 500N lateral force was applied to the front of the head. This motion included the biped raising its one leg forward and then stepping backwards with the same

leg. The biped produced the same motion when the 300N was applied to the front of the head, but differed in terms of the size of the step taken. The GRF angles of the biped when a 500N lateral force was applied to the front of the head is plotted in figure 5.13. After comparison of these angles to the angles from figure 5.10, similarities were noted with respect to the initial nodes. The angles on the first node also ranged between +45 and +90 degrees. However, when the biped is facing the same direction the angles in figure 5.10 and 5.13 will be the opposites of each other.

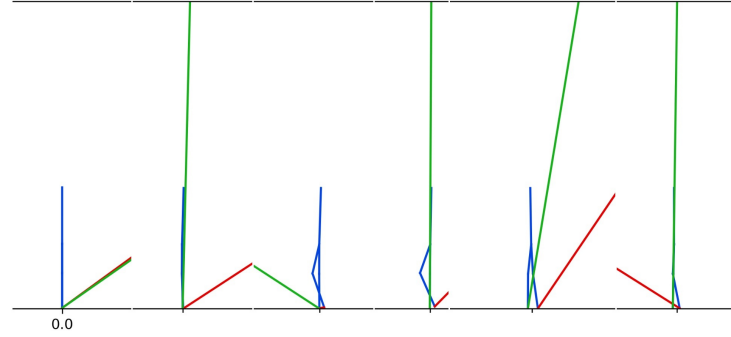


Figure 5.14: 500N lateral force applied at the front of the head - This figure considers the data from a single seed (seed=3) and shows the GRF forces applied to the feet for nodes [1,7,9,17,23,25]. Green represents the left foot's GRF forces and red the right foot's GRF forces. (Note: The magnitudes of the GRF forces were shortened when creating this figure and therefore can not be viewed as accurate.)

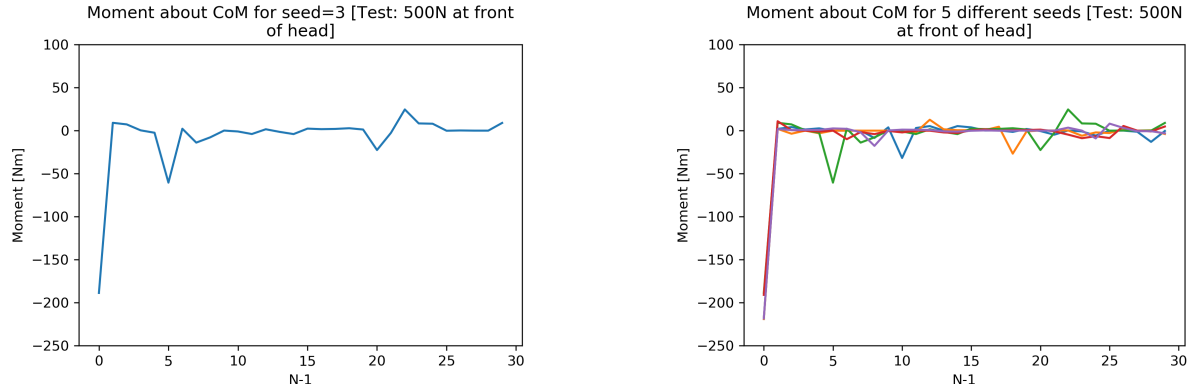


Figure 5.15: These figures show the total moment created by the GRF forces about the CoM of the biped over all 30 nodes. The left figure is the moments for a single seed(seed=3) and the right figure shows the moments for all the seeds.

The animated motion of a single seed (seed=3) with its GRF forces added (refer to figure 5.14) indicated that the disturbance applied at node=1 caused the GRF angles of both feet to start at +45 degrees. This is an indication of the biped's initial attempt to counter the large clockwise moment at node one, shown by the graph on the left in figure 5.15. The leaning forward motion of the biped used at the initial nodes shifted the CoM and ZMP in the negative x-direction which helped reduce the initial disturbance moment but

at the cost of the CoM displacement. Attempting to restore the CoM position to above the feet generated fluctuations in the GRF angles and the moments about the CoM. At node nine the biped reduces these fluctuations by lifting its one leg forwards while leaning back with its body. The +90 angle at node 17 suggests that this technique is effective in restoring the position of the CoM to above the feet in an optimal manner. The biped then finally stepped backwards to recover its original posture.

Additional investigation into the moments about the CoM was done by representing the moments recorded in each head disturbance test as an Gaussian distribution. These distributions are given in figures C.13, C.14, C.15 and C.16. The figures revealed that for each disturbance test there was a unique distribution with regards to the moments about the CoM. The five different seeds simulated in each test had produced similar distributions which suggests that these distributions can be used for identification of different disturbances and the optimal response strategies for them.

5.3. Summary

The above findings show that there is a clear correlation between the angle of the ground reaction forces and the stability of the system. The data collected suggests that there is a balance region with respect to the GRF angles. For all the disturbances simulated the GRF angles never shifted into the following region:

$$-45^\circ \leq \theta_{GRF} \leq 45^\circ$$

This suggests that when the GRF angles move into this range the biped becomes unstable. This supports the idea of the feet having support polygons as discussed in chapter 2. Figure 5.16 illustrates the identified stability regions. The yellow region is the region in which the GRF angles fluctuate when the biped is attempting to balance itself and the green region is when the ZMP is located below the foot and the GRF angle is equal to ± 90 degrees. Note that the GRF angles of both feet have to be located in the green region for the biped to be dynamically stable. The green region for the biped simulated was very small due to the small base of support. Because of the small green region the ZMP of the biped was easily shifted over the edges of the feet for even small disturbances. The small green region also made balance recovery more difficult which is indicated by the rate of fluctuation in the GRF angles.

Apart from the hip- and stepping strategies discussed in chapter 2, additional disturbance response strategies identified in the analysis were the knee strategy and leg-raise strategy. The knee method was always coupled with the hip strategy and

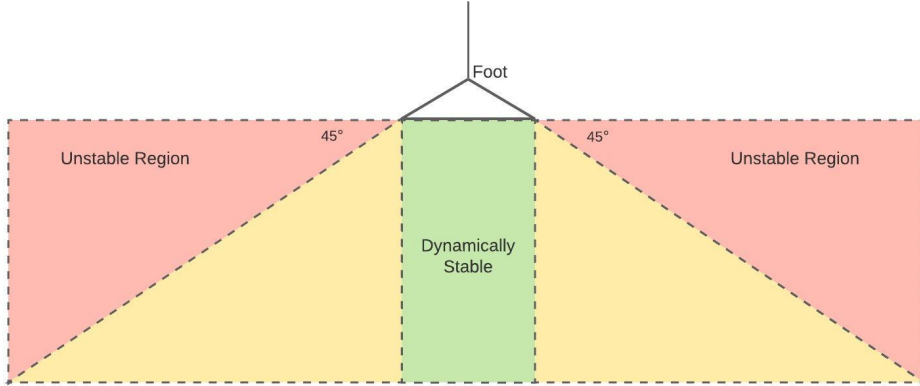


Figure 5.16: The stability regions for the ground reaction forces identified from the simulated results.

included the biped bending its knees to shift the CoM backwards. The leg-raise approach was when the biped raised its one leg forwards or backwards for a period of time before returning it to its original position. This method help create a moment about the CoM and also assisted in shifting the CoM forwards or backwards.

From the analysis it was also proven that the identification of the optimal disturbance response could not be based solely on the GRF angles and it was necessary to consider the magnitudes of the ground reaction forces as well. A simpler approach to help account for both the magnitude and the angle of the GRF when analysing the data was to examine the moments about the CoM. The results, however, proved that moments about the CoM analysis was not suitable for disturbances applied directly to the CoM. For the disturbances not applied to the mid-body the Gaussian distributions of the moments showed promising similarities that could be exploited with the accumulation of more data.

Chapter 6

Analysis and results of biped with added arm

To test whether adding arms to a biped can be beneficial for disturbance rejection, a single link arm was added to the biped and the same disturbance tests as above were simulated. The single link arm had the same length as the body and was modelled as a point mass to help generate larger moments with smaller movements. Figure 6.1 shows a simulated response motion of the new biped when a 1500N disturbance was applied at the back of the mid-body. The figure indicates that the added arm plays an active role in the disturbance rejection and is combined with the hip- and leg-raise strategies. Further investigation showed that the biped initially tried to counter the disturbance by leaning back and shifting its CoM in the negative x-direction. This is indicated by the positive GRF angles at node three. When examining the rest of the motion it was noted that the arm always moved in the opposite direction as the hips. This indicates that the added arm assisted the hip-strategy in shifting the CoM in a more controlled manner. Comparison of the motions in figures C.8 and C.2 showed that the added arm improved the disturbance response motion by reducing the need of a stepping strategy.

The added arm also proved to enhance the response of the biped when a head disturbance

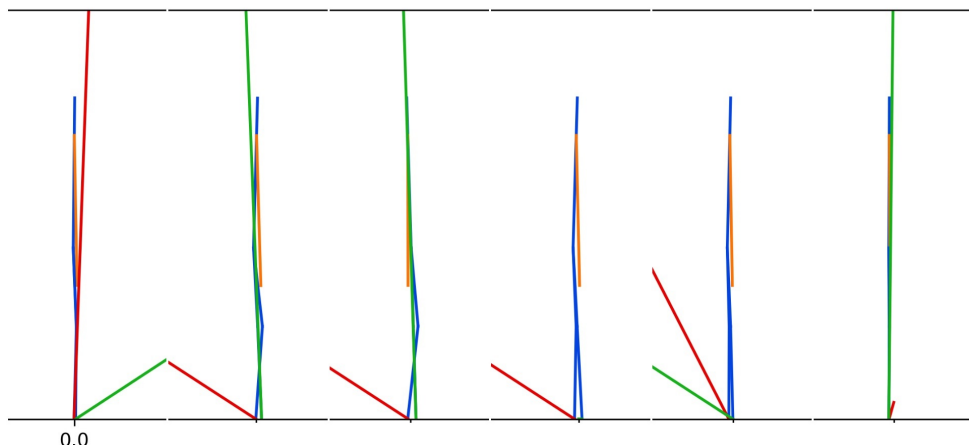


Figure 6.1: The disturbance response motion and ground reaction forces of the biped with the added arm for nodes [3,4,8,14,17,20]. [Test: 1500N applied at the back of the mid-body]

was applied as seen figure 6.2. From the figure it can be noted that at node six the biped shifts its CoM backwards to counter the clockwise moment created by the disturbance. The rest of the nodes showed that the arm was used to assist the hip-strategy in returning the CoM to above the feet in a way that reduces the fluctuation in the moments about the CoM. This was done by extending the arm backwards while the body leaned forwards as seen in nodes 11 and 16 of figure 6.2. When comparing the disturbance response motions in figures 6.2 and 5.11, it was shown that the biped without the arm had to take a step forwards to fully recover from the disturbance, whereas the biped with arm did not require the stepping strategy.

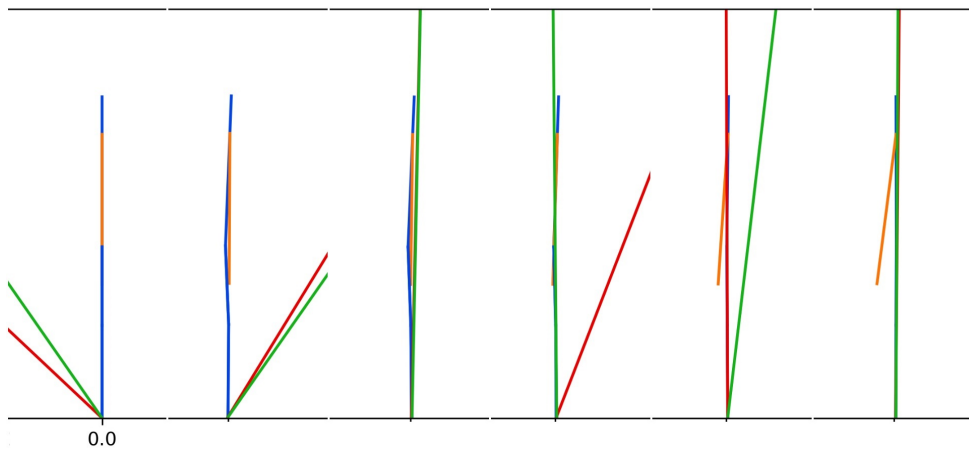


Figure 6.2: The disturbance response motion and ground reaction forces of the biped with the added arm for nodes [1,6,8,9,11,16]. [Test: 500N applied at the back of the head]

From the results above it was noted that the trajectory optimisation algorithm identified arm movements to help reduce the energy consumption of the biped's disturbance response motions. This shows that the results generated from the trajectory optimisation corresponded to the results from other studies (refer to chapter 2) by proving that arms can be beneficial for disturbance rejection in bipeds.

Chapter 7

Conclusion

7.1. Summary

The objective of this dissertation was to investigate the concept of trajectory optimisation being used to help establish optimal disturbance responses for bipedal robots. The investigation focused on optimising the energy consumption of a five-link biped by allowing the trajectory optimiser identify the optimal disturbance response motions. This was done by successfully modelling the optimisation problem as a Pyomo model and then solving the model using the IPOPT solver as discussed in chapters 3 and 4. The analysis of the results in chapter 5 showed that the disturbance response motions chosen by the trajectory optimisation algorithm coincided with the motions described in other literature (refer to chapter 2). Additional biped response strategies identified from the results included the knee- and leg-raise strategies which were very effective in assisting the hip-strategy to control the position of CoM. The GRF angles of the simulated motions also showed trends which proved that the trajectory optimiser had successfully identified the support polygons that are used to determine the stability of the biped as indicated in figure 5.16. Using trajectory optimisation to test whether adding an arm to a biped is beneficial for disturbance rejection was another form of evaluation of the concept. The results generated from the trajectory optimisation proved that the arm was beneficial to the biped's balance and conformed to data collected in other studies (refer to chapter 2).

Similarities noted in the response motions and moments about the CoM of the five seeds generated in each test(refer to chapter 5) indicated that there is potential for developing a criteria that can be used to identify the optimal disturbance responses. Developing a custom criteria based on motions generated from the trajectory optimisation algorithm can be useful for the design of control systems in future bipeds. Therefore, from the evidence stated above it can be deduced that trajectory optimisation can be used to identify and improve disturbance rejection motions of a bipedal robot.

7.2. Future Work

For future studies it is recommended that ankle joints and feet are added to the biped model as this will increase the size of the BoS and will greatly reduce the rate of fluctuation in the GRF angles. If computer performance allows it, the final ϵ tolerance value should also be decreased to improve the accuracy of when ground reaction forces are applied. Increasing the variety and number of disturbance tests performed can also aid in providing more concrete results that can be used to identify trends between different response motions. It is recommended that the position of the CoM with respect to the feet positions is considered in future analysis.

Bibliography

- [1] M. Rouse, “android (humanoid robot).” [Online]. Available: <https://searchenterpriseai.techtarget.com/definition/android-humanoid-robot>
- [2] M. Abdallah and A. Goswami, “A biomechanically motivated two-phase strategy for biped upright balance control,” 05 2005, pp. 1996–2001.
- [3] S.-H. H. . J. G. H. . G. Cheng, “Full-body compliant human–humanoid interaction: Balancing in the presence of unknown external forces,” *IEEE TRANSACTIONS ON ROBOTICS*, vol. 23, no. 5, pp. 884–898, 2007.
- [4] S.-H. H. . G. Cheng, “Disturbance rejection for biped humanoids,” *Computational Brain Project*, 2007.
- [5] C. S. . O. Bruneau, “Robustness of the dynamic walk of a biped robot subjected to disturbing external forces by using cmac neural networks,” High National School of engineering of Bourges, Tech. Rep., 2004.
- [6] F. Plestan, J. W. Grizzle, E. R. Westervelt, and G. Abba, “Stable walking of a 7-dof biped robot,” *IEEE Transactions on Robotics and Automation*, vol. 19, no. 4, pp. 653–668, 2003.
- [7] B. D. . Y. Wang, “Isometric pull-push strengths in workspace: 1. strength profiles,” *International Journal of Occupational Safety and Ergonomics*, vol. 10, no. 1, pp. 43–58, 2004.
- [8] C. Q. Choi, “Brute force: Humans can sure take a punch.” [Online]. Available: <https://www.livescience.com/6040-brute-force-humans-punch>
- [9] A. G. . P. B. . A. L. . R. Vidoni, “Trajectory planning in robotics,” 2012.
- [10] Wikipedia, “Trajectory optimization.” [Online]. Available: https://en.wikipedia.org/wiki/Trajectory_optimization
- [11] M. R. . M. A. Prichici, “Industrial robot trajectory optimization- a review,” *Annual Session of Scientific Papers IMT ORADEA 2017*, vol. 126, 2017.
- [12] L. S. Kaul, “Human-inspired balancing and recovery stepping for humanoid robots,” Ph.D. dissertation, Karlsruher Institut für Technologie (KIT), 2019.

- [13] V. Abadi, M. Rostami, S. M. Rahmati, and S. Sadeghnejad, “Walking path prevision of biped robot along with stability and optimization of power consumption in single support phase,” *Modares Mechanical Engineering*, 10 2017.
- [14] M. Wahde and J. Pettersson, “A brief review of bipedal robotics research,” Chalmers University of Technology, Tech. Rep., 2001.
- [15] J. Pratt, J. Carff, S. Drakunov, and A. Goswami, “Capture point: A step toward humanoid push recovery,” 01 2007, pp. 200 – 207.
- [16] N. T. Pickle, J. M. Wilken, N. P. Fey, and A. K. Silverman, “A comparison of stability metrics based on inverted pendulum models for assessment of ramp walking,” *PLOS ONE*, vol. 13, no. 11, pp. 1–14, 11 2018. [Online]. Available: <https://doi.org/10.1371/journal.pone.0206875>
- [17] A. Hof, M. Gazendam, and W. Sinke, “The condition for dynamic stability,” *Journal of biomechanics*, vol. 38, pp. 1–8, 02 2005.
- [18] M. Nakada, B. Allen, S. Morishima, and D. Terzopoulos, “Learning arm motion strategies for balance recovery of humanoid robots,” *2010 International Conference on Emerging Security Technologies*, vol. 0, pp. 165–170, 09 2010.
- [19] T. Schauss, M. Scheint, M. Sobotka, W. Seiberl, and M. Buss, “Effects of compliant ankles on bipedal locomotion,” in *2009 IEEE International Conference on Robotics and Automation*, 2009, pp. 2761–2766.
- [20] W. S. Rone, Y. Liu, and P. Ben-Tzvi, “Maneuvering and stabilization control of a bipedal robot with a universal-spatial robotic tail,” *Bioinspiration & Biomimetics*, vol. 14, no. 1, p. 016014, dec 2018. [Online]. Available: <https://doi.org/10.1088%2F1748-3190%2Faaf188>
- [21] pdhpe.net, “Base of support.” [Online]. Available: <https://www.pdhpe.net/the-body-in-motion/how-do-biomechanical-principles-influence-movement/balance-and-stability/base-of-support/>
- [22] Wikipedia, “Atlas (robot).” [Online]. Available: [https://en.wikipedia.org/wiki/Atlas_\(robot\)](https://en.wikipedia.org/wiki/Atlas_(robot))
- [23] K. B. Cheng, K.-M. Wang, and S.-Y. Kuo, “Role of arm motion in feet-in-place balance recovery,” *Journal of Biomechanics*, vol. 48, no. 12, pp. 3155 – 3162, 2015. [Online]. Available: <http://www.sciencedirect.com/science/article/pii/S0021929015003851>
- [24] M. Nakada, B. Allen, S. Morishima, and D. Terzopoulos, “Learning arm motion strategies for balance recovery of humanoid robots,” in *2010 International Conference on Emerging Security Technologies*, 2010, pp. 165–170.

- [25] R. Briggs, J. Lee, M. Haberland, and S. Kim, “Tails in biomimetic design: Analysis, simulation, and experiment,” in *2012 IEEE/RSJ International Conference on Intelligent Robots and Systems*, 2012, pp. 1473–1480.
- [26] ExRx.net, “Body segment data.” [Online]. Available: <https://exrx.net/Kinesiology/Segments>
- [27] W. E. Hart, C. Laird, J.-P. Watson, and D. L. Woodruff, *Pyomo - Optimization Modeling in Python*, 1st ed. Springer Publishing Company, Incorporated, 2012.
- [28] C. Fisher, C. Hubicki, and A. Patel, “Do intermediate gaits matter when rapidly accelerating?” *IEEE Robotics and Automation Letters*, vol. 4, no. 4, pp. 3418–3424, 2019.
- [29] C. Fisher, A. Blom, and A. Patel, “Baleka: A bipedal robot for studying rapid maneuverability,” *Frontiers in Mechanical Engineering*, vol. 6, p. 54, 2020.
- [30] S. Dong, Z. Yuan, and F. Zhang, “A simplified method for dynamic equation of robot in generalized coordinate system,” *Journal of Physics: Conference Series*, vol. 1345, p. 042077, nov 2019. [Online]. Available: <https://doi.org/10.1088%2F1742-6596%2F1345%2F4%2F042077>
- [31] M. Kelly, “An introduction to trajectory optimization: How to do your own direct collocation,” *SIAM Review*, vol. 59, no. 4, pp. 849–904, 2017. [Online]. Available: <https://doi.org/10.1137/16M1062569>

Appendix A

Project planning schedule

Weeks	Date	Activity
1,2	29/06/2020 to 13/07/2020	Study literature regarding Lagrange Dynamics, Trajectory Optimisation and Modelling contacts. Start modelling the 5-link biped. Define the generalised coordinates of the model and determine the CoM for each link and apply in python code. Also add the applied actuator torques to the model. Define the potential- and kinetic energies in the code.
3,4,5	13/07/2020 to 03/08/2020	Add code for the GRF and disturbance forces. Add all the necessary bounds and constraints to the code and define the IPOPT solver settings. Also define the cost function in the solver.
6,7,8	03/08/2020 to 24/08/2020	Simulate and store data and amend small issues with the code. Write code that transform the data into comprehensible results.
9,10	24/08/2020 to 07/09/2020	Simulate data for all the disturbance tests. Create separate code for the biped with the added arm.
11,12	07/09/2020 to 21/09/2020	Amend issues with biped+arm code and continue storing simulated data.
13,14,15,16	21/09/2020 to 19/10/2020	Simulate data for the biped with the added arm. Start writing the report. Analyse the data simulated for the 5-link biped.
17,18,19	19/10/2020 to 09/11/2020	Analyse the data simulated from the biped+arm code. Continue writing report.
20	09/11/2020 to 13/11/2020	Make a video presentation of work.

Figure A.1: Planning Schedule

Appendix B

Outcomes Compliance

ECSA Exit Level Outcome	Compliance	Discussion
ELO 1: Problem solving	Code used to simulate results	Multiple problems arose while coding the simulation software and problem solving skills were required to resolve these issues.
ELO 2: Application of scientific and engineering knowledge	Chapter 3,4	The implementation of the biped model and trajectory optimisation algorithms required the understanding of complex mathematics.
ELO 3: Engineering Design	Chapter 3,4	The design of the biped models and the simulation software played a important role in producing feasible results.
ELO 4: Investigations, experiments and data analysis	Chapter 5,6,7	The results produced by the disturbance tests performed as well as the analysis of the results helped answer the research questions. This proves compliance of ELO 4.
ELO 5: Engineering methods, skills and tools, including Information Technology	Chapter 3	The trajectory optimisation algorithms reviewed in this study were implemented with python code and therefore applying python coding skills was essential to produce results.
ELO 6: Professional and technical communication	Report, Video presentation and Q&A meeting	Producing a professional report and video presentation proves compliance of professional communication.
ELO 8: Individual work	Report and Video presentation	The report was written and compiled individually. All the results of this study were only simulated by me.
ELO 9: Independent Learning Ability	Chapter 2,4	Extensive literature on important topics covered in this study as well the implementation of the trajectory optimisation simulation software proves my independent learning ability.

Figure B.1: ECSA Exit Level Outcomes

Appendix C

Additional figures

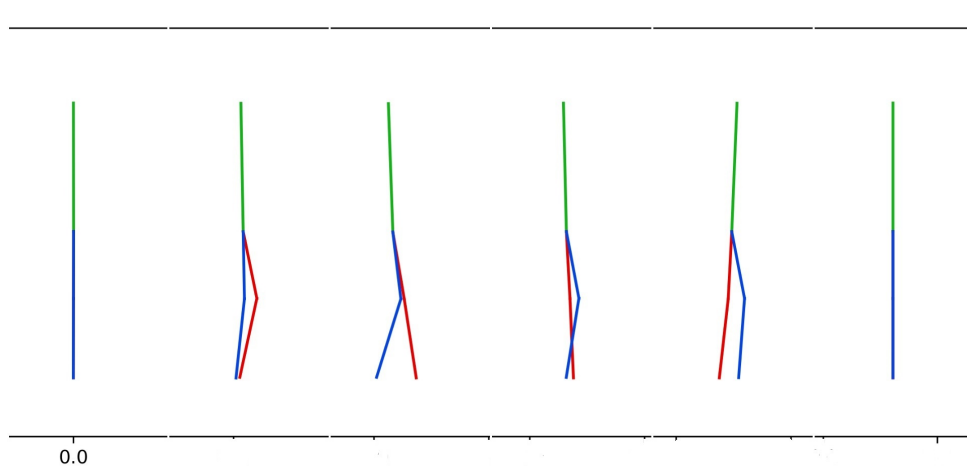


Figure C.1: The typical biped response when a 2000N lateral force applied at the back of the mid-body - The biped takes to two steps to recover from disturbance force and comes to rest at $x_f = 0.1226m$

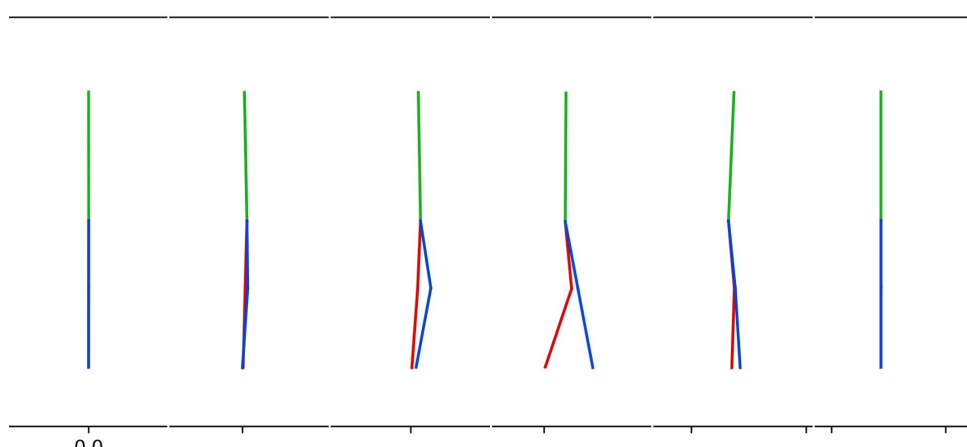


Figure C.2: The typical biped response when a 1500N lateral force applied at the back of the mid-body - The biped takes one step to recover from disturbance force and comes to rest at $x_f = 0.0868m$

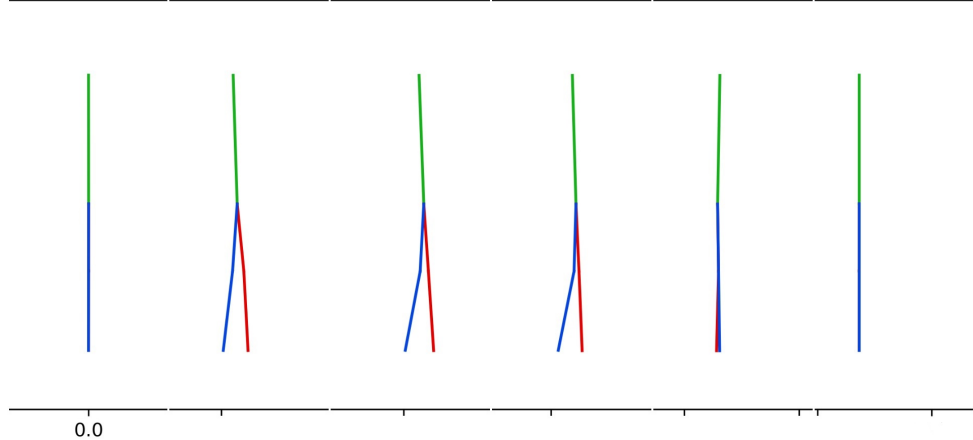


Figure C.3: The typical biped response when a 1000N lateral force applied at the back of the mid-body - The biped takes to one step to recover from disturbance force and comes to rest at $x_f = 0.0731m$

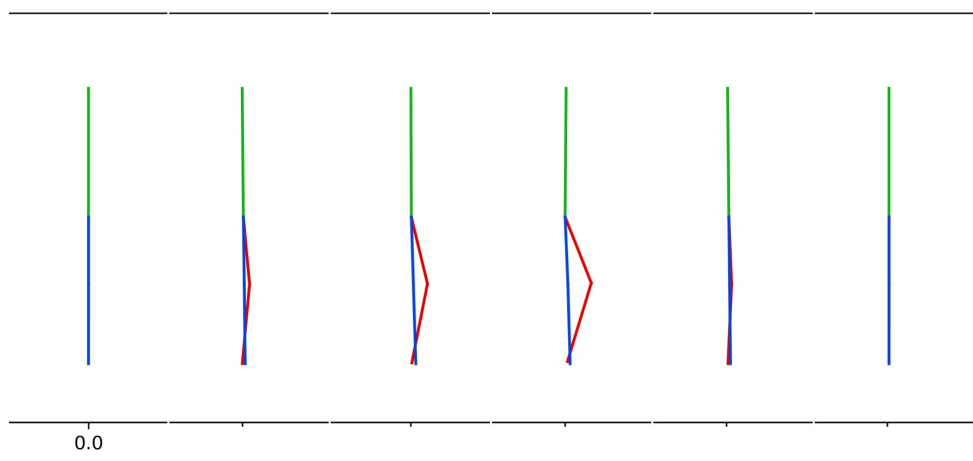


Figure C.4: The typical biped response when a 500N lateral force applied at the back of the mid-body - The biped successfully rejects the disturbance without stepping.

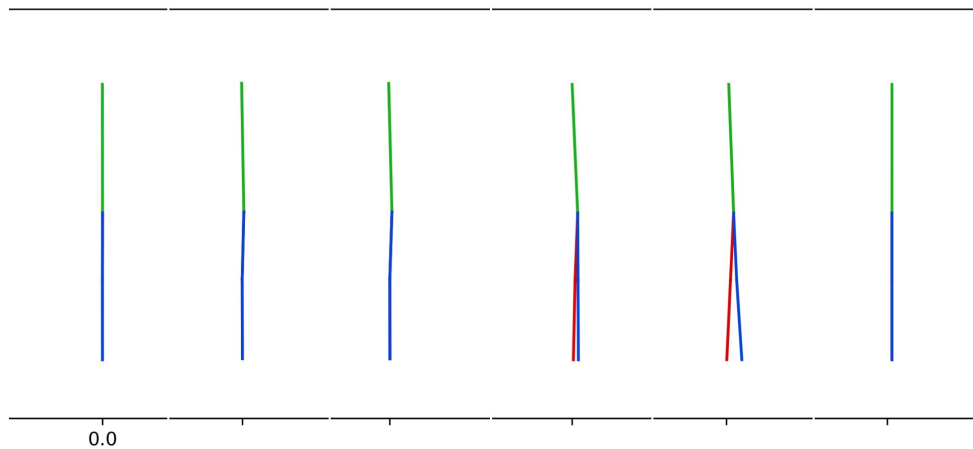


Figure C.5: The typical biped response when a 400N lateral force applied at the front of the mid-body - The biped steps backward a distance of $0.0187m$ with the left leg and then returns to original position.(note: the biped was facing towards the left when mid-body front tests were conducted)

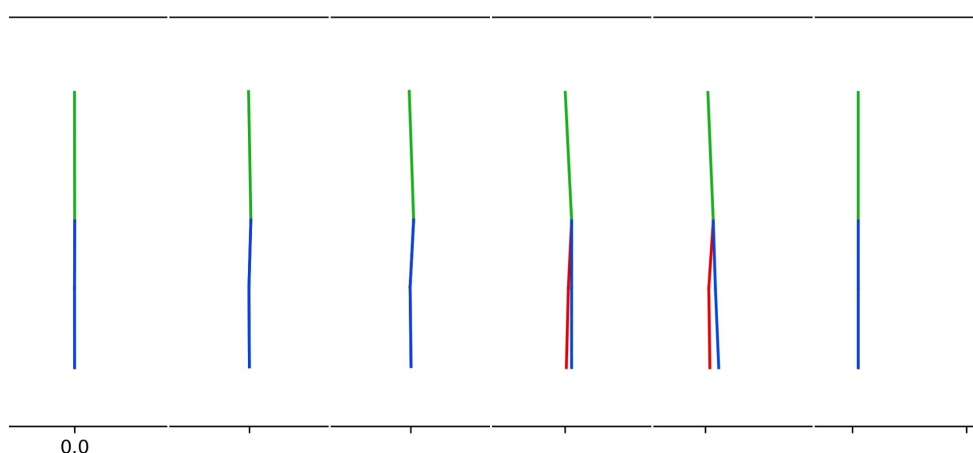


Figure C.6: The typical biped response when a 500N lateral force applied at the front of the mid-body - The biped steps backward a distance of $0.025m$ with the left leg and then returns to original position.(note: the biped was facing towards the left when mid-body front tests were conducted)

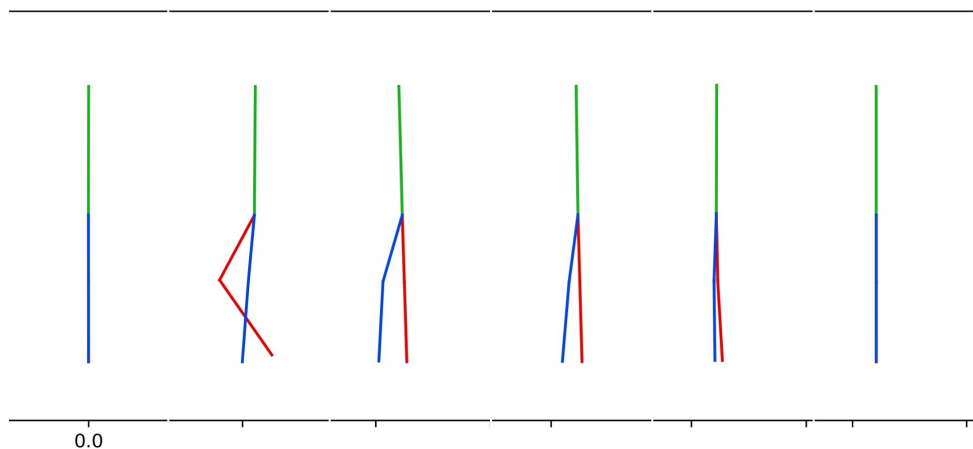


Figure C.7: The typical biped response when a 500N lateral force applied at the front of the head - The biped takes one step backwards to recover from disturbance force and comes to rest at $x_f = 0.042m$.(note: the biped was facing towards the left when mid-body front tests were conducted)

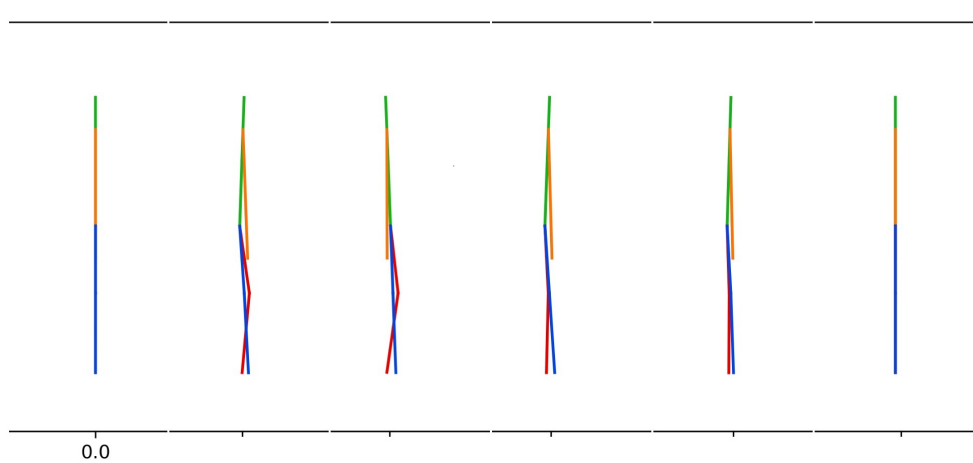


Figure C.8: Simulated disturbance response motion of the biped with a single link arm added. [Test: 1500N applied at the back of the mid-body]

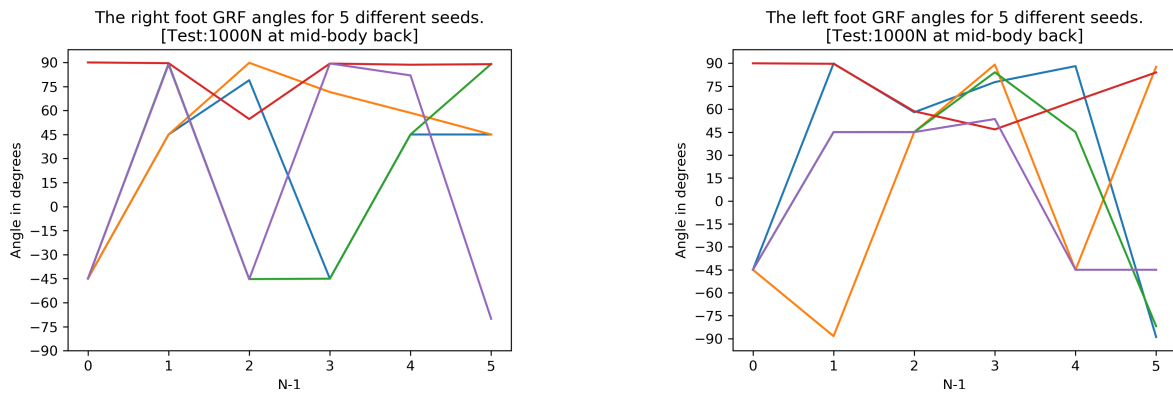


Figure C.9: Ground reaction force angles of the right and left foot for the first six nodes when 1000N lateral force is applied at the back of mid-body.

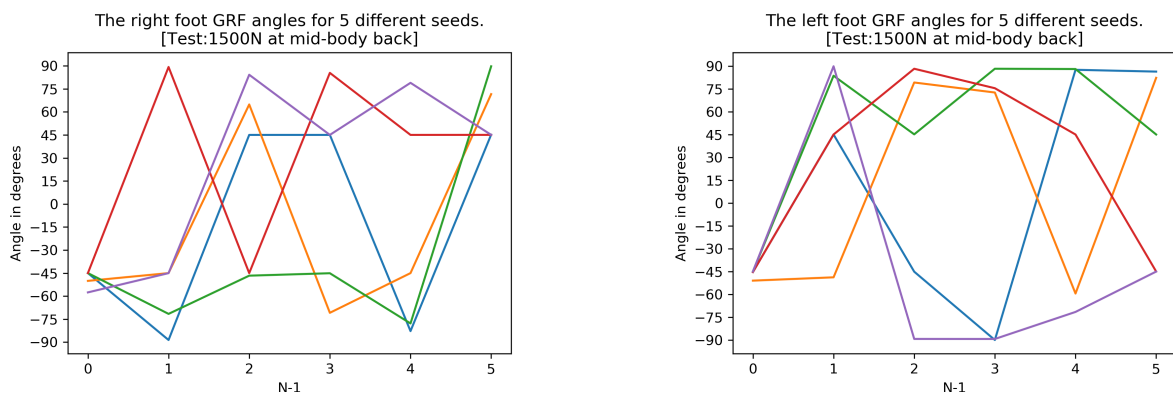


Figure C.10: Ground reaction force angles of the right and left foot for the first six nodes when 1500N lateral force is applied at the back.

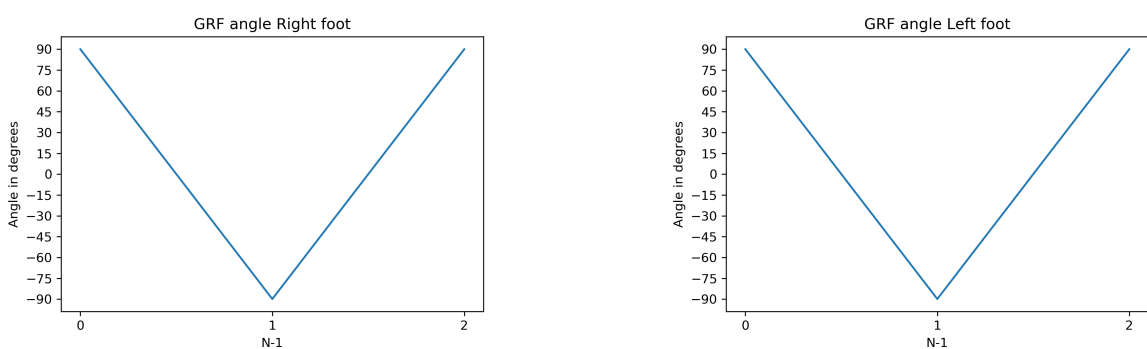


Figure C.11: Ground reaction force angles of the right and left foot for the first three nodes when no disturbance force is applied.

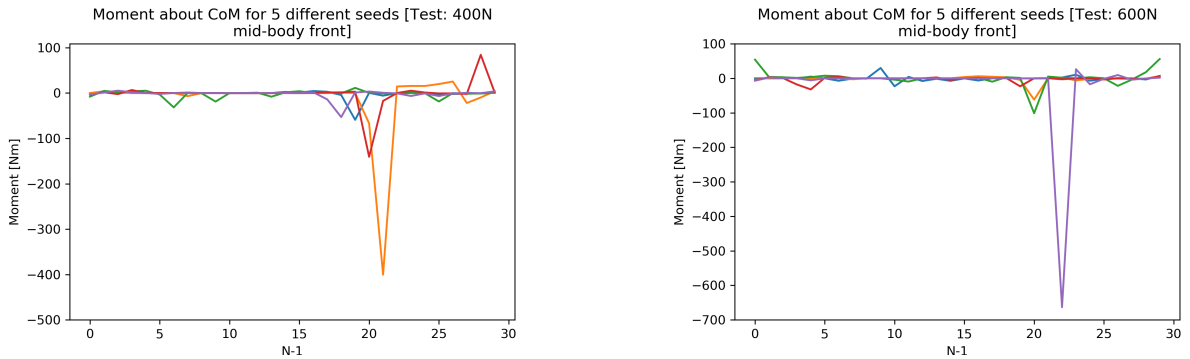


Figure C.12: These figures show the total moment created by the GRF forces about the CoM of the biped over all 30 nodes.

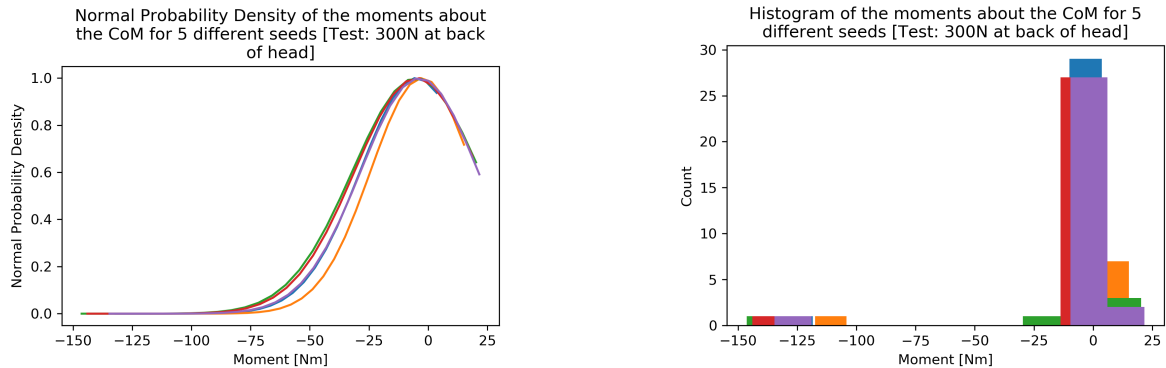


Figure C.13: [Test: 300N applied to the back of the head] The two graphs above show the normal distribution and histogram of the moments about the CoM for five different seeds simulated. The moments of all 30 nodes are represented in the graphs.

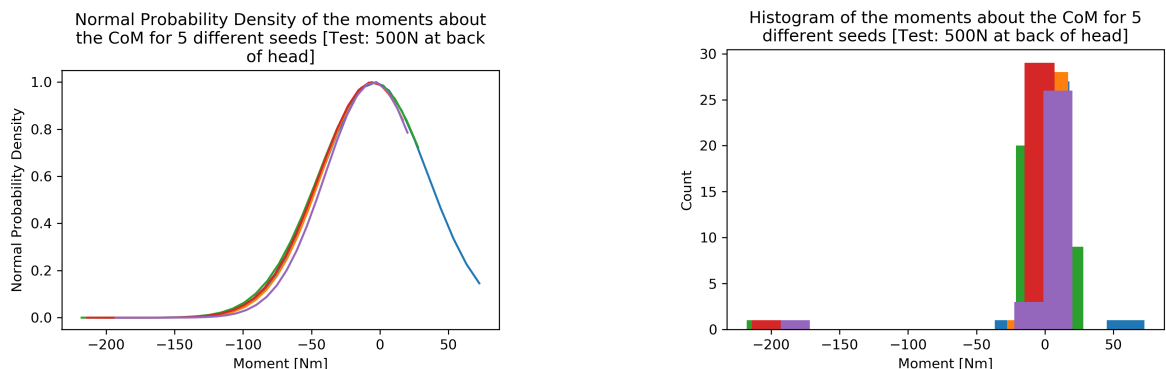


Figure C.14: [Test: 500N applied to the back of the head] The two graphs above show the normal distribution and histogram of the moments about the CoM for five different seeds simulated. The moments of all 30 nodes are represented in the graphs.

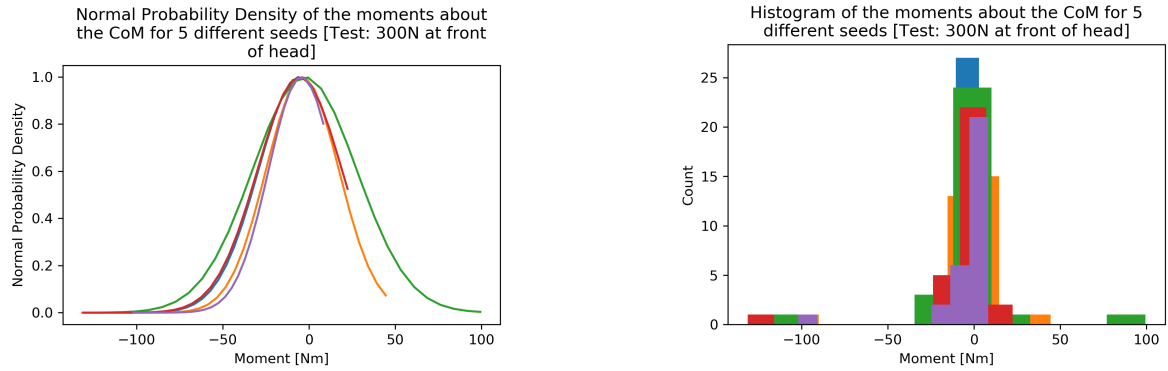


Figure C.15: [Test: 300N applied to the front of the head] The two graphs above show the normal distribution and histogram of the moments about the CoM for five different seeds simulated. The moments of all 30 nodes are represented in the graphs.

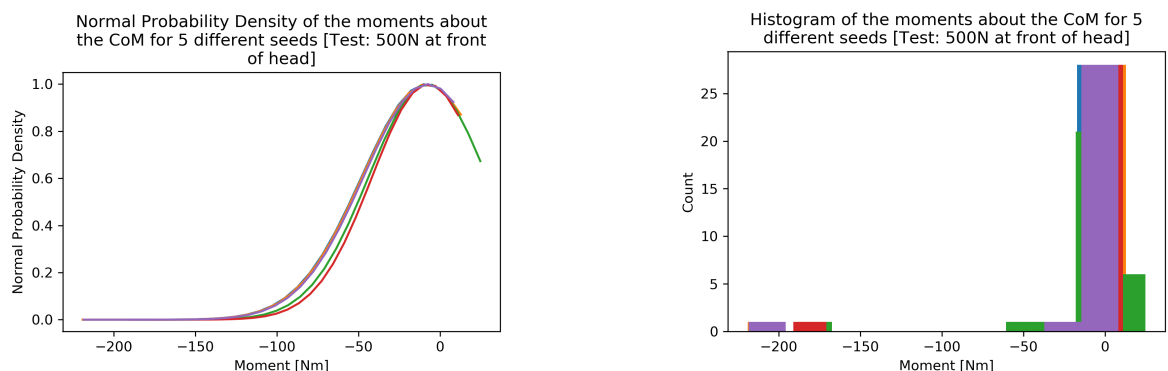


Figure C.16: [Test: 500N applied to the front of the head] The two graphs above show the normal distribution and histogram of the moments about the CoM for five different seeds simulated. The moments of all 30 nodes are represented in the graphs.